RAMAN STUDIES ON THE ALUMINATE AND CARBONATE ANIONS IN AQUEOUS SOLUTIONS

YIXIN ZHOU

Raman Studies on the Aluminate and Carbonate Anions in Aqueous Solutions

By

Yixin Zhou

A thesis submitted to the School of Graduate Studies in partial fulfilment of requirements for the degree of Master of Science

Department of Chemistry
Memorial University of Newfoundland
St. John's, Newfoundland, Canada

May 1995

ISBN 0-612-06164-7

Canada

Abstract

Sodium aluminate solutions and their precipitates have been investigated by Raman spectroscopy. All Raman data are consistent with the existence of $Al(OH)_4^-$ and $Al_2O(OH)_6^{2-}$ anionic species in sodium aluminate solutions. In supersaturated solutions, both anions are in equilibrium during the induction process. After the induction period, sodium aluminate solutions produce a precipitate which contains neither the $Al(OH)_4^-$ anion nor the $Al_2O(OH)_6^{2-}$ anion.

Quantitative Raman studies with 0.23 M $NaNO_3$ as an internal standard were employed to elucidate the equilibria in sodium aluminate solutions. The best values of the molar scattering constants J_i are equal to 0.25±0.03 for the $Al(OH)_4^-$ and 0.57±0.18 for the $Al_2O(OH)_6^{2-}$ species relative to the 1.0 M NO_3^- ionic mode at 1052 cm^{-1}. With these J_i values the formation quotient Q and equilibrium constant K are estimated.

In addition, studies of the effects of temperature on the Raman frequencies and halfwiths of CO_3^{2-}, $Al(OH)_4$ and $Al(OD)_4$ anions in H_2O and D_2O reveal evidence for the presence of strong hydrogen bonds between these anions and water. There is no significant change in the hydrogen band strength at temperatures up to 150°C.

Acknowledgements

I would like to take this opportunity to thank my supervisors, Drs. Murray H. Brooker and Peter R. Tremaine, for their continued support and patient guidance throughout this work.

Financial support from Memorial University of Newfoundland is gratefully acknowledged.

CONTENTS

List of Tables

List of Figures

Symbols and Definitions

Symbols	Definitions
a_i	Activity
A_i	Raman band area of species i
A.C.	Alternating Current
C_i	Concentration of species i
CARS	Coherent Anti-Stokes Raman Spectroscopy
CCD	Charge-Coupled Device
D.C.	Direct Current
E	Electric field
FT-Raman	Fourier Transform Raman
h	Planck constant
I	Ionic strength
I_{mn}	Raman intensity
IR	Infrared
J_i	Molar scattering constant of species i
k	Boltzmann constant
K	Equilibrium constant
M	Molarity (moles per litre of solution)
n	vibrational quantum number
NMR	Nuclear Magnetic Resonance

P	Electric dipole moment
Q	Formation Quotient
Q_v	Normal vibrational coordinate
RRS	Resonance Raman Spectroscopy
PMT	Photomultiplier
SERS	Surface Enhanced Raman Spectroscopy
T	Temperature
t	Time
α	Polarizability
γ	Activity Coefficient
μ	The reduced mass
ν	Frequency
ρ	Degree of polarization
Ψ	Vibrational wave function

Chapter 1. Introduction

Many important chemical reactions which are carried out in laboratories or in industry, or which occur in living organisms take place in aqueous solutions. To understand the mechanism and thermodynamics of these chemical reactions, it is necessary to know what species are present and how the solute-solute, solute-water and water-water interactions affect solute properties.

Within the last three decades, spectroscopic techniques such as Raman[1-4], IR[4,5], NMR[6,7] and X-ray diffraction[8] have been systematically applied to resolve many structural and dynamical problems in solution chemistry.

Raman spectroscopy is in theory an ideal technique to study aqueous solutions. Water is a poor Raman scatterer and the Raman spectra of solutes and their complexes are easily separated from that of the water solvent. Glass is transparent to visible laser light and it is relatively easy to construct cells to study samples under a variety of different conditions including low and high temperatures or pressures. There is a considerable variety of excitation sources, detectors, ancillary data processing and handling equipment, and sampling cells and geometry. All these devices are relatively inexpensive and readily available from equipment vendors, or these can be specially constructed. Problems such as low Raman scattering efficiency,

spectroscopic complications due to broad bands, overlap bands, Fermi-resonance, overtones, and coloured samples become solvable with the rapid advance of optical, electronic and computer techniques. Therefore, important information on aqueous solutions can be obtained. Perhaps the most valuable information obtained from Raman spectroscopy is the identification of discrete species. Quantitative analyses of band intensities and shapes over a wide range of concentration, temperature and pressure can provide rich information on chemical equilibria, reaction rates, ion hydration, ion pairs and hydrogen bonds.

1.1. Objectives

The principal aim of this work has been to obtain new information concerning anionic aluminate species, the induction process, precipitation products, J values (molar scattering constants), equilibria and information related to hydrogen bonds in aqueous sodium aluminate solutions. Hydrogen bonding to hydrated carbonate anions in aqueous carbonate solutions was also studied. Although such information is of fundamental interest, the systems studied were also chosen to give insight into the chemical processes occurring during the production of aluminum, and some industrial and geochemical processes.

1.2. The Hydrolysis of Aluminum in Caustic Aqueous Solutions

Aluminum is the most abundant metal in the earth's crust (8.3% by weight). Aluminum occurs only in the oxidized form, Al(III). In caustic aqueous solutions the anionic species are mainly $Al(OH)_4^-$ [6,9,10] with tetrahedral structure and its condensed product $Al_2O(OH)_6^{2-}$[10-13]. However evidence from NMR[9] and Raman experiments[11,12] has led some researchers to propose that a small concentration of the $Al(OH)_6^{3-}$ species exists in highly caustic solutions.

The distribution of anionic species in caustic aqueous solutions is a function of ionic strength, the total aluminum concentration, the hydroxide concentration, and temperature. So far, hydrolysis constants for several monomeric and polymeric cationic complexes have been reported at elevated temperatures. However, due to experimental difficulties, the only hydrolysis constant obtained for an anionic species at temperatures above 100°C is that of the monomer, $Al(OH)_4^-$. These investigations correspond to aluminum concentrations and ionic strengths from 10^{-5} to 10^{-2} M and 0 to 5.0 M respectively[6,14].

It is well known that supersaturated aqueous aluminate solutions may be easily obtained by dissolving aluminium metal or aluminium hydroxides in concentrated aqueous hydroxide solutions. After preparation, supersaturated solutions may initially remain clear but precipitates form

after an induction period. The rates of formation and composition of the precipitates may depend on the temperature, the pH, the amount of crystalline solid already present, and perhaps on the other cations or anions present in the solutions. Johansson[15], and Moolenaar et al.[10] have shown, from X- ray diffraction, Raman and IR spectra of their precipitates, that $K_2Al_2O(OH)_6$ forms in aqueous potassium aluminate solutions. Ivekovic et al.[16] found that the density and viscosity of sodium aluminate solutions oscillate in the induction period. Recently Chen et al.[12] also found that supersaturated aqueous sodium aluminate solutions with the same composition but different preparative histories may exhibit quite different optical and NMR spectra during the induction period. They also observed slow interconversion between anions in solutions of different $Al(OH)_3$(aq.)/NaOH(aq.) ratios.

1.3 Hydrogen Bonds to Hydrated Carbonate and Aluminate Anions

Vibrational spectroscopy provides the ideal technique to study ion hydration. For cations such as Mg^{2+}, Cu^{2+}, Al^{3+}, Fe^{3+} etc. hydration may be measured directly by the observation of Raman bands in the 250-550 cm^{-1} range caused by the M-O stretching vibrations of the hydrate or indirectly by changes in the Raman and IR spectra of the hydrated water[1,5]. For

anions such as hydroxide, fluoride and carbonate, direct evidence of hydration has been obtained from the observation of new bands in the 200 to 300cm^{-1} region in Raman spectra[1]. Indirect evidence for anion hydration has also been detected through changes in the Raman and IR spectra of water[1,5]. However the new bands and spectral features of water caused by the hydrated ions are very weak and it is difficult to use these features to study the effects of temperature and concentration on ion hydration.

Recently the systematic differences in the frequency shifts and halfwidths between hydroxy-complexes or oxyanions and their deuterated analogues[17,18] have been used to provide information on hydrogen bonding. Prelimentary work has examined aqueous $Al(OH)_4^-$, $B(OH)_3$, $B(OH)_4^-$, $Zn(OH)_4^-$ and CO_3^{2-} at room temperature. The vibrational intensities of carbonate and aluminate anions are relatively strong. So studies of the effect of temperature on hydrogen bonding to these anions become possible.

1.4. Scope

This thesis deals mainly with an examination of sodium aluminate solutions and carbonate solutions in H_2O and D_2O using Raman spectroscopy.

In the next chapter, there is a brief review of the theory of conventional Raman spectroscopy. In Chapter 3, the

instrumentation for conventional Raman spectroscopy is described.

Chapter 4 is devoted to the Raman studies on aluminate anions in aqueous solutions, including determinations of anionic aluminate species, the induction process, precipitation products, the molar scattering constants J_i, formation quotients Q and equilibrium constant K.

Chapter 5 consists of a review of the systematic differences in the Raman frequency shifts and halfwidths of the carbonate and aluminate anionic modes in H_2O and D_2O at room temperature. An examination of their behaviour as a function of temperature reveals strong evidence of the hydrogen bonding of water to carbonate and aluminate anions even at high temperature.

Chapter 2. Theory of Conventional Raman Spectroscopy

2.1. Short Historical Review

A rapid development of the quantum mechanical theory of light scattering took place in the early 20th century. The radiation scattered from molecules contains not only photons with the frequency of the incident light but also photons with a changed frequency (Raman effect) due to interactions with molecular vibrations. This effect was first predicted by Smekal[19] in 1923, then by Kramers and Heisenberg[20] in 1925, Schrödinger[21] in 1926, and Dirac[22] in 1927. In 1928 this prediction was confirmed by experimental observations with liquid benzene by Raman[23]. Almost at the same time this phenomenon was also discovered in a quartz crystal by Landsberg and Mandelstan[24]. In 1930 Raman was awarded the Nobel prize and the phenomenon he discovered is given his name.

After Raman spectroscopy was born, it became a principal method of non-destructive analysis before the Second World War. By 1939 a vast range of liquids, a few gases, one or two polymers and crystals had been analyzed. However, following the Second World War, highly sensitivity infrared detectors became available and, these, coupled with advances in electronics, made the development of automatic infrared

spectrometers possible. By comparison, Raman spectroscopy in its early stage with the need for a powerful mercury vapour discharge lamp as light excitation source, a conventional spectrograph as light dispersive system and photographic plates as detector remained a slow and tedious procedure for any type of sample.

Great progress in Raman spectroscopy resulted from the invention of lasers in the mid-1960s. Since that time, and with the development of holographic gratings, specialized electronic equipment and especially the application of Fourier transform techniques, Raman spectroscopy has matured to a flexible, analytical technique. Now there are numerous recognized variants of Raman scattering such as normal Raman, surface enhanced Raman, stimulated Raman, induced Raman, hyper-Raman, inverse Raman, resonance Raman, coherent anti-Stokes Raman, Raman gain, Raman induced Kerr-effect, etc. The development and application of Raman theories and techniques have become a branch of spectroscopy. For example, Surface Enhanced Raman and Resonance Raman spectroscopies have been employed to study the structure and function of catalysts and biological molecules at very low concentrations[25,26]. Coherent Anti-Stokes Raman spectroscopy has been applied to studies of combustion processes at high temperature and pressure[26]. Because all of these applications of Raman scattering phenomena have the potential to be performed under conditions similar to those employed in actual reaction environments

during chemical processing, Raman spectroscopy has become more and more popular as a standard technique in academic and industrial labs.

As only conventional Raman spectroscopy was employed in our work, the theory of normal Raman scattering will be briefly described. For specialized Raman theories such as Coherent Anti-Stokes Raman Spectroscopy (CARS), Resonance Raman Spectroscopy (RRS), Surface Enhanced Raman Spectroscopy (SERS), etc, the readers can refer to references 25-29.

2.2. Classical Theory[30,31]

An electric dipole moment **P** is induced within a molecule when an electromagnetic wave having an electric field **E** is impinging upon the molecule. For small electromagnetic fields, this induced dipole can be represented by:

$$\boldsymbol{P}=\alpha\boldsymbol{E} \tag{2.1}$$

α is a tensor and is called the polarizability.

Eq. (2.1) implies that the relationship between the **P** and **E** vectors can be placed into the matrix form:

$$\begin{pmatrix} P_x \\ P_y \\ P_z \end{pmatrix} = \begin{pmatrix} \alpha_{xx} & \alpha_{xy} & \alpha_{xz} \\ \alpha_{yx} & \alpha_{yy} & \alpha_{yz} \\ \alpha_{zx} & \alpha_{zy} & \alpha_{zz} \end{pmatrix} \begin{pmatrix} E_x \\ E_y \\ E_z \end{pmatrix} \tag{2.2}$$

The above matrix is symmetric; that is, $\alpha_{ij} = \alpha_{ji}$.

The electromagnetic radiation generates an electric field which can be expressed as:

$$\mathbf{E}=\mathbf{E}_o \cos 2\pi\nu_o t \tag{2.3}$$

$\mathbf{E}_o$ is the maximum electric field strength and ν_o is the angular frequency of the radiation.

In this case, the induced dipole moment will fluctuate in time as:

$$P_i=\sum_j \alpha_{ij} E_{oj} \cos 2\pi\nu_o t \tag{2.4}$$

where P_i is the ith component of electric dipole moment $\mathbf{P}$ and E_{oj} is the jth component of the maximum electric field strength $\mathbf{E}_o$.

If we let Q_v represent some normal vibrational coordinate of the molecule and consider the harmonic approximation, we can expand the polarizability in terms of Q_v as

$$\alpha=\alpha_o+\left(\frac{\partial\alpha}{\partial Q_v}\right)_o Q_v \tag{2.5}$$

The coordinate Q_v is a function of time and may be written as

$$Q_v=Q_v^\circ \cos 2\pi\nu_v t \tag{2.6}$$

where Q°_v is the maximum distortion and ν_v is the frequency of the v th vibration. Upon substitution of Eqs. (2.5) and (2.6) into Eq. (2.4) we obtain

$$P_i = \sum_j (\alpha_o)_{ij} E_{oj} \cos 2\pi \nu_o t + \frac{1}{2} \sum_j E_{oj} Q_v^o \left(\frac{\partial \alpha_{ij}}{\partial Q_v} \right)_o \times [\cos 2\pi (\nu_o + \nu_v) t + \cos 2\pi (\nu_o - \nu_v) t] \qquad (2.7)$$

The first term in Eq. (2.7) describes the process that radiates light of the same frequency as the incident radiation, i.e. Rayleigh scattering. The second term of Eq. (2.7) describes the effect of dipoles oscillating at frequencies $\nu_o + \nu_v$ and $\nu_o - \nu_v$ called anti-Stokes and Stokes Raman scattering.

It is seen from Eq. (2.7) that Raman scattering will not occur unless the derivative term $(\partial \alpha_{ij} / \partial Q_v)_o$ is nonzero. In other words, the polarizability of the molecule must change during a vibration if that vibration is to be Raman active.

2.3. Quantum Theory I: Time-Independent[25,31]

A molecule of N atoms has 3N-6 normal modes of vibration (3N-5 if linear). If we only consider the harmonic approximation, the energy of each of these vibrations will be quantized according to the relationship:

$$E_i = h\nu_i \left(n + \frac{1}{2} \right) \qquad (2.8)$$

where ν_i is the frequency of the vibration and n is the

vibrational quantum number (0,1,2,...).

Using the Dirac notation, the requirement of a non-zero vibrational transition moment $(P_i)_{ab}$ is given by:

$$(P_i)_{ab}=\langle\psi_a|P_i|\psi_b\rangle\neq 0 \qquad (2.9)$$

where $\psi_{a,b}$ are final (b) and initial (a) states of the system's vibrational wave function, and P_i is the i th component of the induced moment operator as indicated in Eq.(2.1). Hence, in terms of the ij polarizability component, and with substitution of the Eq.(2.5), Eq.(2.9) can be written as:

$$(\alpha_{ij})_{ab}=(\alpha_o)_{ij}\langle\psi_a|\psi_b\rangle+\left(\frac{\partial\alpha_{ij}}{\partial Q_v}\right)_o\langle\psi_a|Q_v|\psi_b\rangle \qquad (2.10)$$

This equation can be used to define whether α_{ij} components will be zero. For example, vibrational, harmonic oscillator functions are orthogonal, implying that the first term (Rayleigh scattering term) of Eq.(2.10) is non-zero only if the quantum numbers do not change; that is, $n_a=n_b$. For the second term, the condition of non-zero values becomes $n_b = n_a \pm 1$ of the vibrational quantum numbers.

For small molecules, the requirement that the partial derivative of the polarizability at the molecular equilibrium configuration be non-zero is easy to assess. For larger molecules, this requirement is less easy to determine. However, Raman activity also can be assessed by looking at

the components of the symmetric tensor (α_{ij}). From Eqs.(2.2) and (2.9), the condition for Raman activity could be written:

$$(\alpha_{ij})_{n_a\ n_b} = \langle \psi_b(Q_v) | \alpha_{ij} | \psi_a(Q_v) \rangle \neq 0 \qquad (2.11)$$

This requirement implies a non-zero integral if α_{ij} and $\psi_b(Q_v)$ belong to the same symmetry species; that is, under each symmetry operation of the molecule being investigated, the α_{ij} and $\psi_b(Q_v)$ transform in the same manner. Eq.(2.11) is a consequence of a harmonic oscillator assumption. However, the consequence of this equation in terms of Raman activity is independent of whether the wavefunctions are anharmonic or harmonic representations. Group theory must be applied to the molecule for predicting Raman activity[30,32,33].

2.4. Quantum Theory II: Time-Dependent, First Order Perturbation Theory[25,31]

To obtain the electric dipole transition moment associated with the vibrational transition from an initial state (a) to a final state (b), the Hamiltonian of a molecular system can be considered to contain only an electric dipole term and be subject to the perturbation of an electromagnetic field at frequency ν_o. The restriction of using only an electric dipole interaction term does not limit the validity of the solution for the case in which the electric field intensity does not vary over the length of the

molecule. Here, in contrast to previous time-independent solutions, the transition moment is found to be a complex number, the real part of which can be written as

$$(\alpha_{ij})_{ba}=\frac{1}{h}\sum_{r}\left[\frac{(P_j)_{br}(P_i)_{ra}}{(\nu_{ra}+\nu_o)}+\frac{(P_i)_{br}(P_j)_{ra}}{(\nu_{ra}-\nu_o)}\right] \qquad (2.12)$$

where the summation is over all of the energy states (r) of the system. Because the transition moments in Eq.(2.12) always occur as products, there must exist in the system at least one state r that has a non-zero dipole transition moment to both the initial and final states. This statement and Eq.(2.12) do not imply that the transition from the initial state (a) to the final state (b) occurs in two distinguishable states, that is, via an intermediate state (r). Also, Eq.(2.12) does not imply the absorption of energy $h\nu_o$ during the transition from (a) → (b), as there is no requirement to have $h\nu_r = h\nu_o$. The state (r) can be higher in energy, lower in energy, or between the state (a) and (b) in energy. The useful pictorial description of these transitions may be shown in Figure 2.1.

Rayleigh scattering arises from transitions which start and finish at the same energy level. Stokes Raman scattering arises from transitions which start at the ground state energy level and finish at a higher energy whereas anti-Stokes Raman scattering involves a transition from a higher to a lower energy level. According to the Boltzman

distribution law, molecules are generally much more populated at ground energy level. Hence Stokes Raman scattering is more intense than anti-Stokes'. For this reason Stokes Raman scattering is usually used in Raman spectroscopy.

Incorporation of time dependence in the transition moment calculation shows that there will be a phase difference in the scattering between one molecule and the next. Hence, Raman scattering will be spatially and temporally incoherent. On the other hand, no phase difference will exist for Rayleigh scattering; that is, it is coherent scattering. In addition, although the formalism of Eq.(2.12) involves any energy level (r) that must have a non-zero dipole transition moment with both initial and final states, the selection rule for Raman vibrational activity can be written in terms not involving the properties of state (r). For example, it can be shown that $(\alpha_{ij})_{ba}$ has the same transformation properties as $\langle b,ij,a\rangle$. Hence, the general condition of having a non-zero such as $\langle\Psi_b,xy,\Psi_a\rangle \neq 0$ belongs to a representation that contains totally symmetric species.

2.5. Selection Rules

Among the 3N-6 normal modes of vibration (3N-5 if linear) of a molecule with N atoms, only those modes with a change in the polarizability of the molecule are Raman active whereas only those modes with a change in the dipole moment of the

molecule are Infrared active. Some vibrational modes, however, are not observed in Raman or IR spectroscopy because they have no effect on either the molecular polarizability or dipole moment.

For small molecules, it is possible to visualize the change of the molecular polarizability and the dipole moment against the progress through the vibration, Q_v, and determine whether or not it is Raman and IR active. But, for a more complex molecule, it become difficult. An alternative method of classifying fundamental vibrations is required.

As described in the preceding section, Raman activity depends on non-zero contributions of the integral of the type: $\langle \Psi_b, ij, \Psi_a \rangle$, where ij = xy, yz, and so on. Hence molecular symmetry dictates the number and activity of Raman vibrational modes. The determination of Raman activity (also of IR activity) is greatly facilitated by considering the equilibrium symmetry of the molecule of interest and applying the methods of group theory. The detailed description of group theory can be found in many books[30, 32, 33].

For the free molecule, when its point group has been determined, character tables which list all the symmetry elements can be used to label fundamental modes of vibration using irreducible representations according to their symmetry and to predict Raman and IR activity. A vibration is Raman active if it has the same irreducible representation as a component of the polarizability. These are represented by x^2,

y^2, z^2, xy, xz, yz or a combination of products such as $x^2 - y^2$, indicated in the character table. A vibration is infrared active if it has the same irreducible representation as a component of dipole moment. These are shown by the x, y and z labels in the character table. One important consequence of the selection rules is the so-called rule of mutual exclusion: if the molecule is centrosymmetric, normal modes which are Raman active will not be IR active and vice versa. This result can be seen directly from the character table.

The results from point group theory are exact in describing the symmetries of the normal modes and predicting their spectral activities when the molecules are in a dilute gaseous state. The method can be used for less ideal systems, such as liquids and solutions, but some disagreement between prediction and observation may occur. The procedure used with free molecules usually shows poorest agreement with solid systems. Indeed, molecules in a gas are randomly oriented and essentially free of intermolecular or interionic perturbations, but in the condensed state this is no longer true. Here, the orientation of the molecules is such as to minimize the free energy. This leads to an infinite regular repetition in space of identical structural units. In the solid state, the actually symmetry of the molecule in the crystal (site symmetry) and the symmetry of the crystal lattice itself (space group symmetry) must be taken into consideration[34,35].

The whole method of applying group theory to vibrational problems depends upon the fact that normal modes of vibration have special symmetry properties because the wavefuctions that describe them should remain invariant under the possible symmetry operations. These properties are identical to the properties of certain species of the factor group. Thus, Raman (or IR) active modes of a crystal will be determined by the factor group. The correlation of the symmetry species representing the ionic vibrational modes through the site group, to the factor group, limits the number of possible factor groups. For an unknown structure, polarization measurements, the frequency and the number of Raman (and IR) modes measured can elucidate possible factor groups to which a crystal may belong.

2.6. Raman Intensity

Many efforts have been made for the derivation of Raman intensity from the semi-classical and quantum mechanical theories. For brevity, only the semi-classical Raman intensity based on Placzek's polarizability is described here[30,31].

It is seen from Eq.(2.7) that Raman intensity is related to the derivative, $\alpha'_{ij} = (\partial\alpha_{ij}/\partial Q_v)_o$. In order to express the scattering intensity in terms of the derived polarizability tensor, it is necessary to find quantities which are

constants regardless of the orientation of the molecule. These invariants are found to be:

Mean value of the polarizability:

$$\bar{\alpha}=\frac{1}{3}(\alpha'_{xx}+\alpha'_{yy}+\alpha'_{zz}) \tag{2.13}$$

The polarizability anisotropy:

$$\bar{\gamma}=\frac{1}{2}[(\alpha'_{xx}-\alpha'_{yy})^2+(\alpha'_{yy}-\alpha'_{zz})^2 + (\alpha'_{zz}-\alpha'_{xx})^2+6(\alpha'^2_{xy}+\alpha'^2_{xz}+\alpha'^2_{yz})]^{\frac{1}{2}} \tag{2.14}$$

Now we can consider the use of these invariants to express the intensity of Raman scattering. If we consider randomly oriented non-rotating molecules with a singlet ground state which conforms to the Born-Öppenheimer approximation and excitation light with the frequency ν_o that is much less than any electronic frequency of the molecule, the Raman intensity of a Stokes band with the frequency shift ν_i from an initial vibrational state (m) to a final state (n) over a solid angle of 4 π is given by:

$$I_{mn}=\left(\frac{2^7\pi^5}{3^2C^4}\right) I_o(\nu_o-\nu_i)^4 \sum_{ij} |(\alpha_{ij})_{mn}|^2 \tag{2.15}$$

where I_o is the incident intensity, c the speed of light and α_{ij} the components of the polarizability tensor associated with the transition from (m) to (n).

With the substitution of Eq.(2.10) into Eq.(2.15), the total Raman intensity of a Stokes band arising from N molecules can be obtained from averaging over all molecular orientations and is given as:

$$I_{mn}=\left(\frac{2^4\Pi^3}{3^2c^4}\right)\frac{hNI_o(\nu_o-\nu_i)^4}{\mu\nu_i\left[1-\exp\left(\frac{-h\nu_i}{kT}\right)\right]}\sum_{ij}\left|\left(\frac{\partial\alpha_{ij}}{\partial Q_{mn}}\right)_o\right|^2 \qquad (2.16)$$

where h and k are Planck's and Boltzman's constants respectively. Q_{mn} is the normal vibrational coordinate between state (m) and (n) where m = n ± 1.

Using Eqs.(2.13) and (2.14) and combining all constants as K in Eq.(2.16), we have:

$$I_{mn}=\frac{KNI_o(\nu_o-\nu_i)^4}{\mu\nu\left[1-\exp\left(\frac{-h\nu}{kT}\right)\right]}\left(45\bar{\alpha}^{\,2}+7\bar{\gamma}^{\,2}\right) \qquad (2.17)$$

where μ is the reduced mass of the oscillator.

2.7. Polarizability[30,31]

Not only are the frequencies and intensities of Raman lines important in elucidating molecular structure but the study of the polarization properties of the scattering light is found to be very important. Specifically, polarization studies can be used to help determine the symmetries of the

vibrations involved.

Consider incident unpolarized light propagating in the y direction and scattering in the x direction (90° scattering geometry) as shown in Figure 2.2. As the degree of polarization is defined as $\rho_n = I_y/I_z$, averaging over all molecular orientations this depolarization ratio is found to be

$$\rho_n = \frac{6\bar{\gamma}^2}{(45\bar{\alpha}^2 + 7\bar{\gamma}^2)} \tag{2.18}$$

Using incident plane polarized light it is easily shown that

$$\rho_p = \frac{3\bar{\gamma}^2}{(45\bar{\alpha}^2 + 4\bar{\gamma}^2)} \tag{2.19}$$

where the subscript (p) denotes polarized incident light. If $\rho_p = 0.75$, the line is said to be depolarized; if $\rho < 0.75$, the line is polarized; and if $\rho_p = 0$, the line is completely polarized. The value of the depolarization ratio can be used to assist in the determination of the symmetry of vibrations. This can be done because the poilarizability can be associated with an isotropic, or spherical, part $\bar{\alpha}$ and an anisotropic part $\bar{\gamma}$. The isotropic portion is related to the change in size of the polarizability ellipsoid, while the anisotropic part is related to the change of orientation of the ellipsoid.

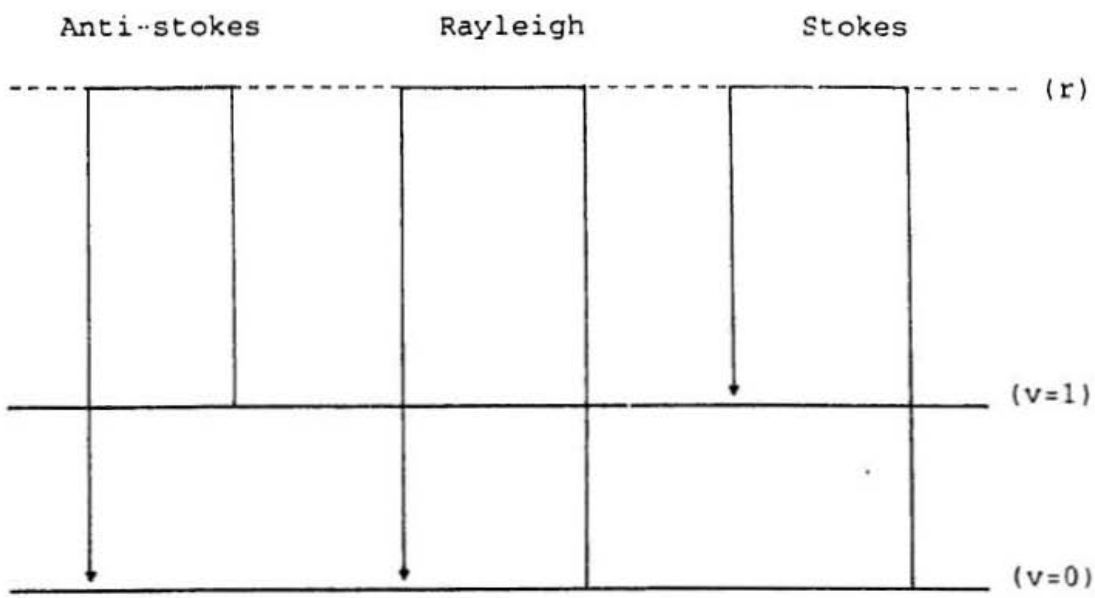

Figure 2.1. Pictorial Description of Transitions for Rayleigh and Raman Scatterings

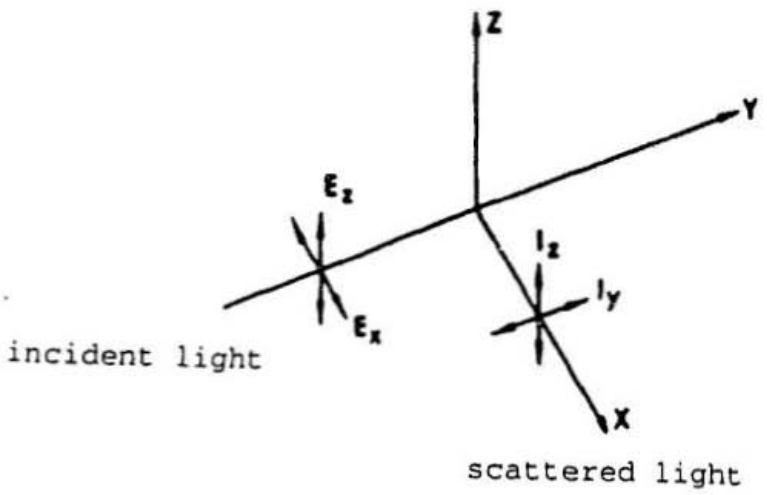

Figure 2.2. Polarization of Scattering for Unpolarized Incident Light

Chapter 3. Instrumentation for Conventional Laser-Raman Spectroscopy

The conventional laser-Raman system consists of: (1) a laser source; (2) sample chamber; (3) optical system; (4) monochromater; (5) detector; (6) amplification, display and record system and (7) computer system. A schematic diagram of a typical (Coderg PHO) laser-Raman spectrometer is shown in Figure 3.1.

3.1. Lasers

Raman scattering can be generated by an excitation source of any wavenumber. In order to study a wide variety of samples it is desirable to have several laser wavelengths available. This may enable the user to reduce problems of sample heating and fluorescence, by switching from one excitation source to an alternative. In modern Raman spectroscopy, in addition to argon laser (488.0, 514.5nm etc.), He-Ne (632.8 nm) and Krypton lasers, tunable (dye) lasers (visible region) have been popularly employed as excitation sources. In recent years, the Nd-YAG laser (1.06um) has also been employed with a FT-Raman spectrometer[36].

3.2. Sample Chamber

For Raman spectroscopy, sampling is simple and flexible. Because solids, liquids and gases need only be enclosed in a vessel which is transparent to the laser and Raman scattered light, as a result, a host of simple cells for innumerable experiments have been devised[36]. For example, quartz tubes, pyrex tubes, glass sample bottles, flasks, ampoules and some polymer tubes/or containers may be directly used as sample cells for liquid and solution samples. In special cases, rotating and circulating cells equipped with motor and pump can be used in order to overcome the catastrophic heating of the sample by the laser.

Thermostat and pressure apparatus can also be employed in the sample chamber. With the use of strong cells such as diamond anvils[37,38] high temperature and pressure studies are also possible.

3.3. Optical system

The optical system mainly includes a set of collimating and collecting lens/mirrors which bring the laser beam to focus either inside the sample or on its surface, collect and focus the scattering radiation into the entrance slits of a monochromater. In general, 90° and 180° scattering arrangements are used in experiments (Figure 3.2). When a

microscope is used at the front of a Raman spectrometer, the microscope objective lens acts in both focusing the laser beam on the sample and collecting and focusing the Raman scattered light into the monochromator[16].

The optical system also includes a polarizer and scrambler for depolarization measurements, an interference filter or foremonochromater for removing other plasma lines of lasers, and neutral density filters or iris diaphragms for reducing the laser intensity. Some additional optical components may be added in special cases.

3.4. Monochromator

The monochromator contains dispersive elements, generally holographic gratings, whose number depends on the amount of discrimination needed for separating the highly intense Raleigh scattering. Monochromaters with two diffraction gratings are very popular in Raman spectroscopy. A monochromater with three gratings may increase the resolution ability and reduce the background caused by Raleigh and Tyndall scattering in the sample. But it also loses part of Raman scattering.

The principle of the double momochromater is shown in Figure 3.1. Light enters the device through a narrow slit and is reflected and dispersed by five mirrors and two diffraction gratings. The sixth mirror then reflects this

light onto an exit slit. Two gratings actually produce a series of images of the entrance slit on the exit slit plane, each displaced by the wavelength of the radiation entering the instrument. However, only one of these images can pass through the exit slit and onto the detector. This image can be viewed either by having a wide exit slit and using a multichannel detector, or by rotating the grating and tracking the image across a narrow exit slit to produce a spectrum.

At this time the dispersive instruments still hold a dominant position in conventional Raman spectrometry. However, the dispersive instrument has been replaced by the Fourier transform interferometers employed in FT-Raman spectrometers in recent years. FT-Raman spectrometers have become commercially available. The principle of interferometry is quite different from monochromaters. For detailed information about interferometers, the reader is referred to reference 36.

3.5. Detectors

There are two types of detection systems, i.e. single channel and multichannel, in Raman spectroscopy. In single channel, perhaps the ultimate detector for visible and ultraviolet light is the modern high-performance photomultiplier tube (PMT)[39]. Light falls on the front face

of the detector, which is an electrically charged photocathode. Electrons are produced as a result of the photoelectric effect, and these are accelerated towards a series of dynodes at which more electrons are produced. Each dynode serves to increase the electron current and the device acts as an 'electron amplifier'. Typically PMT's contain up to 14 dynodes, so the gain of the device is very high. A single photon event at the photocathode produces a large, easily measured pulse at output. Unfortunately spontaneous emissions occur from the photocathode, so these tubes give an output of a train of pulses even in the dark. This so called dark current or dark count can be reduced by cooling the tube, and many Raman spectrometers incorporate PMT refrigeration designed to reduce the temperature to approximately -40°C.

Photomultipliers are invariably used in scanning instruments, and the radiation leaving the exit slit is focused onto the photocathode by a simple lens as the frequency is scanned (Figure 3.1). As previously mentioned, multichannel analyzers are also popularly used because of the increased speed with which spectra can be acquired, as compared to the speed with the use of photomultipliers. In multichannel instruments, the detector has to be large and segmented, so that the intensity at each discrete frequency can be monitored separately and continuously. The maximum spectral resolution with multichannel analyzers is inferior to that achieved with photomultipliers.

Recently, several different types of multichannel analyzers have been applied in Raman spectroscopy. Initially, photodiode arrays and sensitive TV cameras (vidicon)[40] were used in conjunction with imagine intensifier. Latter, more sensitive photodiode arrays[40] and charge coupled devices (CCD)[41] have been developed, and these make excellent Raman detectors.

3.6. Application, Display and Record Systems

The output pulse train for a quantum detector such as a photomultiplier is analyzed by either (1) a direct current (D.C.) amplifier (2) an alternating current (A.C.) amplifier with a chopper in the laser beam, causing it to pulse at a desired frequency, or (3) photon counting electronics. The third amplifier device is the most popular one in Raman spectroscopy. Some spectrometers (e.g. the Coderg PHO, Cary 82) are equipped with two electronic systems, i.e. a D.C. amplifier and a photon counter, which can be used interchangeably.

Photon-counting electronic systems consist of an energy discriminator followed by either a ratemeter, a scaler counter, or a suitably interfaced microcomputer fast enough to monitor individual pulses. The discriminator which acts as an energy gate is set to pass counts large enough to originate from electrons leaving the photocathodes, but

reject those emanating accidentally further along the dynode sequence. Where a counter is used, its output is normally made available for subsequent processing in digital form after each sample period and Raman spectrum is simultaneously displayed on computer screen or recorder with a drive mechanism operating the grating rotation and record chart jointly or independently. All digital data can be stored in a computer and the Raman spectrum can be plotted on a plotter from these data.

The electronic pulse outputs of multichannel analyzers can be simultaneously converted into digital data by complex electronic circuits and the Raman spectrum is displayed on an oscilloscope or a screen of a computer. All digital data can be stored in a computer and plotted by a plotter.

3.7. Computer system

In a modern Raman spectrometer, laser parameters are still controlled by hand. The computer is normally used to control the monochromater and detector parameters, display the Raman spectrum and to store and treat the digital Raman data.

Modern Raman spectrometers are normally supplied with a dedicated computer and a software package to operate the spectrometer or perform a range of operations on the acquired data. The major advantage offered by computer processing is

the ability to make optimum use of the photons collected and to store and display the spectra, as well as to smooth noise and record weak bands which is realized through multiple scanning and spectral entrancement. Further advantages are automatic measurement of band position and intensity and the possibility of simultaneous determination of other qualities, such as band area, the concentrations of components of mixtures, and molecular constants. An additional facility is the comparison of a spectrum of a substance with spectra stored in the memory of a computer.

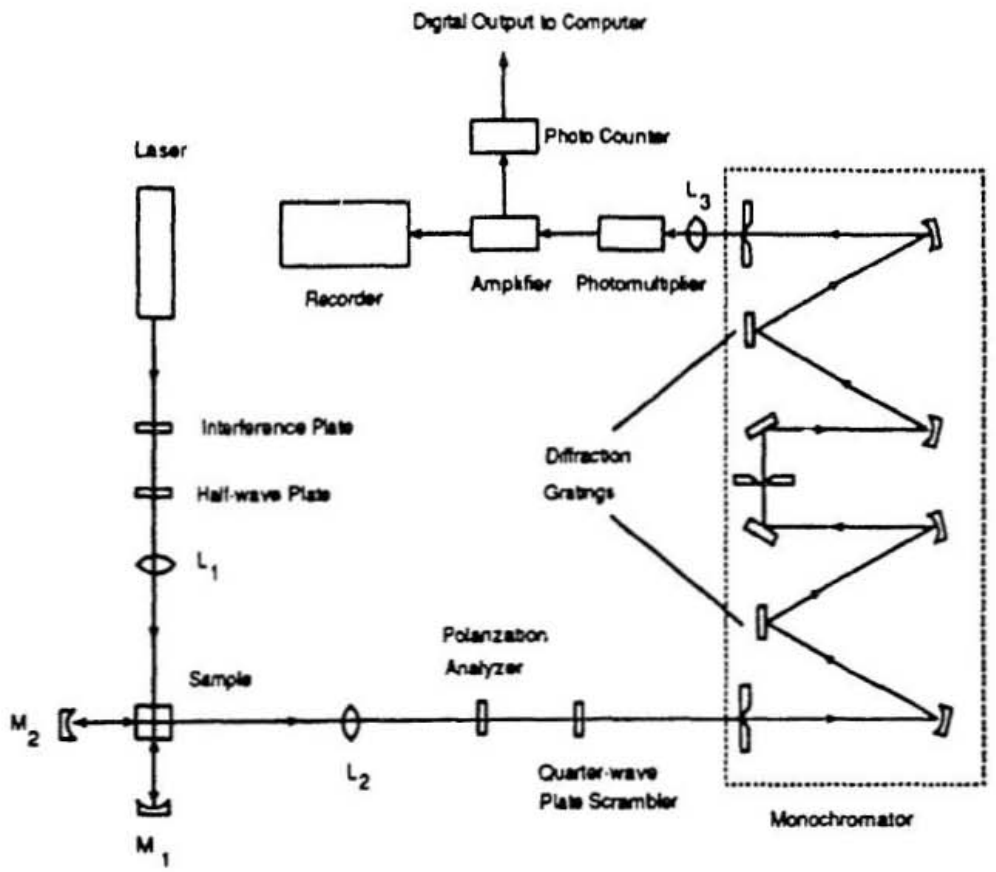

Figure 3.1. Schematic Diagram of the Coderg PHO Raman Spectrometer

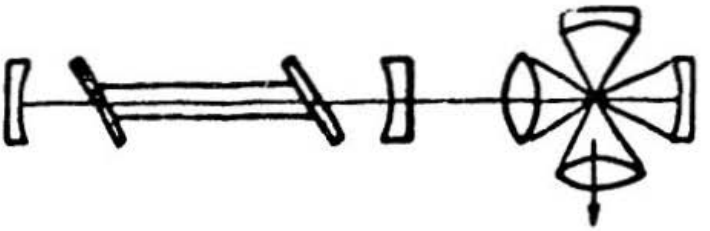

a.

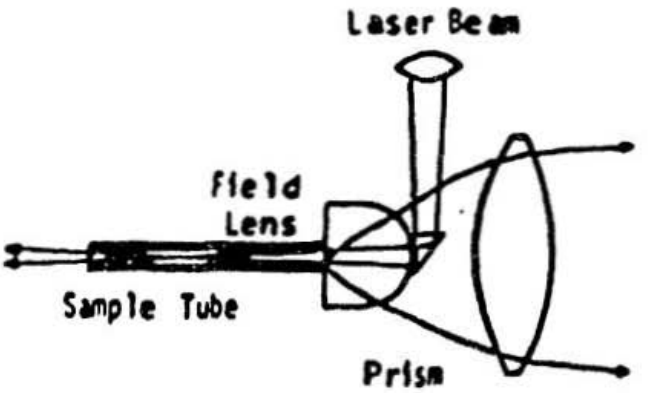

b.

Figure 3.2. (a.) 90° and (b.) 180° Scattering Arrangements

Chapter 4. Studies on Aluminate Anions in Aqueous Solutions

4.1. Introduction

The dissolution of gibbsite, γ-$Al(OH)_3$, in aqueous NaOH serves as a key step in the extractive metallurgy of aluminum. Therefore knowledge of the anionic aluminate species, induction process, precipitation products, and equilibria of aqueous aluminate solutions is very important for the understanding of many chemical reactions in aluminium production.

The stability and structure of anionic aluminate species are of fundamental importance in an understanding of the physical chemistry of aluminum production. In early Raman and NMR studies it was concluded that tetrahedral $Al(OH)_4^-$ and $Al_2O(OH)_6^{2-}$ anionic species were present in caustic aqueous solutions[6,13]. However, later Raman and NMR studies in highly caustic aqueous solutions led some workers to postulate the existence of another anionic aluminate species, $Al(OH)_5^{2-}$[9,11,12]. Sufficient controversy exists to warrant further investigations of species formation on a more quantitative basis.

Highly caustic and concentrated aluminate solutions are encountered in the Bayer process of aluminium production. Although the solubility of aluminum hydroxides is low[14,42] these solutions are often supersaturated because precipitates do not form when the hot solutions cool. The solutions will be in

metastable equilibrium for the induction period required to nucleate the solid phase that precipitates. However, the speciation in the metastable solutions and the mechanism of nucleation are still poorly understood. Ivekovic et al.[16] found that the density and viscosity of sodium aluminate solution oscillated in the induction period. Chen et al.[12] also found chaotic oscillatory changes in the UV and Raman spectra occurred in the induction period. So far, no quantative studies have been reported in the literature to elucidate the equilibration of supersaturated solutions during the induction process.

In addition, the precipitation products from the caustic aluminate solutions are interesting. Johasson[15], and Moolenaar et al.[10] have shown, from X-ray diffraction, Raman and IR studies, that $K_2Al_2O(OH)_6$ formed from the precipitation of aqueous potassium aluminate solutions, but the nature of the precipitate formed from sodium aluminate solutions is still not clear.

In this chapter, our qualitative and quantitative Raman studies of sodium aluminate solutions will be described.

4.2. Experimental

4.2.1. Preparation and Analyses of Sodium Aluminate Solutions

Highly concentrated sodium aluminate solutions No.6 - No.16 were prepared in polyethylene flasks by dissolving a weighed

amount of reagent grade γ-Al(OH)$_3$ (gibbsite) and NaOH in water with constant stirring. Cosiderable heat was produced and supersaturation was possible. The pH values of solutions No.8 - No.16 were around 15. More dilute solutions were prepared by dilution of concentrated sodium aluminate solutions with dilute sodium hydroxide. Pure water was not used because dilution of concentrated sodium aluminate solutions with water caused slight precipitation. Solutions from No.1 to No.7 had a 1:4.1~4.4 mole ratio of Al(OH)$_3$(aq.) to NaOH(aq.). We note that carbon dioxide gas dissolves in sodium aluminate solutions to produce carbonate ion. In order to prevent atmospheric gases from reacting with sodium aluminate solutions the solutions were kept in air-tight polyethylene bottles under N_2 gas after quick filtration through a fine sintered glass frit etc. Solution prepared from γ-Al(OH)$_3$ in the high pH region (>10) appeared to be much less soluble than predictions made from published solubility and hydrolysis constants in dilute solutions and the assumption of the stability of γ-Al(OH)$_3$ and exisitence of one anionic species $Al(OH)_4^-$ in sodium aluminate solution[14,42]. This is because, as we will be seen later, the precipitate produced in sodium aluminate solutions is no longer γ-Al(OH)$_3$ and a second species $Al_2O(OH)_6^{2-}$ is also formed in these solutions. All aluminate solutions studied in our work were nominally supersaturated but remained clear and colorless at room temperature for one

week or more, depending on the concentrations of aluminum and hydroxide.

The aluminum concentrations in the concentrated solutions were determined gravimetrically by precipitation as the 8-hydroxyquinolate salt[43]. Hydroxide was determined by titration with HCl to pH 7 at which point all of the aluminate is precipitated as γ-$Al(OH)_3$ (gibbsite) [44]. For quantitative Raman studies, sodium nitrate (0.23 M) was included in all solutions since the N-O stretching band at ~ 1052 cm^{-1} was found to be a useful internal standard for intensity calibrations. The solution compositions investigated are listed in Table 4.1.

The samples of solid precipitates for Raman studies were obtained by decanting precipitates from sodium and potassium aluminate solutions. The solid samples were stored in a vacuum desiccator with desiccant to keep them water free.

4.2.2. Raman measurement and data treatment

Raman spectra were measured using a Coderg PHO Raman spectrometer equipped with an Ebert-Fastie double grating, twin monochromator, a single-channel PH 100 photo-counting unit connected to a VAX 8800 computer system, and a Coherent INNOVA 70-4 argon ion laser operating at approximately 1 W at the 488.0 nm line. The scattering Raman radiation was detected at an angle of 90° with respect to the exciting

beam. Slits corresponding to ca.4 cm^{-1} for solutions and 2 cm^{-1} for solids were used. The wavenumber accuracy was 0.5 cm^{-1}. The wavenumber repeatability was 0.1 cm^{-1}. The maximum resolution was 1.0 cm^{-1}. A narrow-band pass interference filter was used to remove plasma lines near the 488.0 nm line. The PMT was cooled to ~ -30°C. The scan rate was chosen as 50 cm^{-1} min^{-1} and the total counts were collected for the time interval that corresponds to a 0.5 cm^{-1} spectral interval.

Quartz tubes were used as sample cells. Before sampling, the tubes were leached using concentrated sodium hydroxide solution. With this treatment, the reaction rates of the solutions with the quartz tubes became much slow and the quality of Raman spectra were greatly improved, especially for the solutions with high caustic ratios. For the high temperature measurement the quartz tube was sealed by a high temperature flame. Solid samples were also sealed in vacuum quartz tubes to avoid deliquescence.

All samples were measured three times and their Raman data were stored on the VAX 8800 computer. Spectra were averaged and smoothed twice with a Savitsky-Goly three-point smoothing function[45]. A baseline program was applied which corrects the measured intensity for the fourth power scattering factor and set the lowest point as 0 and the highest point as 999 on the relative scale. For solid samples the reduced version of the Raman spectra in the low

wavenumber region was used[45]. The spectra of sodium aluminate solutions contain an exponential background and very weak broad bands due to Rayleigh scattering and the presence of hydrated sodium ion. These were treated by subtracting the spectra of aqueous solutions of NaOH to form a flat baseline and normalized by using the integrated area of the N-O symmetric stretching band of 0.23 M $NaNO_3$ at 1052 cm^{-1} as the internal standard. A curvefit program, which was originally developed by Pitha and Jones[46,47] for Infrared spectroscopy and subsequently modified by Brooker and Rice[48] for Raman spectroscopy, was used to estimate areas of the component bands. The relative integrated molar scattering molar intensities and concentrations of scattering species were calculated from the Raman data by the regression method through the program SIGMA PLOT[49].

4.3. Results and Discussion

4.3.1. Determination of anionic species

Our Raman spectra of sodium aluminate solutions No.1 - No.16 at room temperature are shown in Figs.4.1 and 4.2. Spectra are concentration dependent, the intensity changes being consistent with the presence of a predominant aluminate species at lower concentration of aluminum, and a second

species whose relative concentration increases as the concentrations of aluminium and NaOH are increased. All Raman bands observed for the low and high concentration solutions, e.g. solutions No.1 and 7, are listed in Table 4.2.

$Al(OH)_4^-$ species: In lower concentration solutions, our Raman spectra (Fig.4.1 and 4.2) suggest that the predominant species is $Al(OH)_4^-$. The observed spectra reveal a strong Al-O symmetric stretching mode (ν_1) at ~620 cm^{-1}, the weak AlO_4 antisymmetric bending modes (ν_2, ν_4) at ~325 cm^{-1} and a weak AlO_4 antisymmetric stretching mode (ν_3) at ~710 cm^{-1}, which are consistent with the results from R. J. Moolenaar et al.[10]. The Raman band at ~620 cm^{-1} is highly polarized with a value of the depolarization ratio that is barely distinguishable from zero. Two other bands at ~320 and 710 cm^{-1} are depolarized. All Raman bands for the $Al(OH)_4^-$ species are listed in Table 4.3.

^{27}Al-NMR spectra[6,9,10] obtained at 25°C show a strong resonance line at 80 ppm downfield from the $Al(H_2O)_6^{3+}$ resonance. The large negative chemical shift of the ^{27}Al in basic solution, as compared to that for octahedral Al^{3+} in acid solution, suggests a coordination number less than 6 for the aluminate ion. The best interpretation is that the predominant species is tetrahedral $Al(OH)_4^-$, which agrees with the NMR results for solid compounds containing Al-O tetrahedra[50].

The experimental Raman data confirm that the aluminate anion, $Al(OH)_4^-$, is the principal species in caustic solutions and it displays approximately cubic symmetry although the hydroxy groups of tetrahedral structure are strongly hydrogen bonded to water[17]. The depolarization ratio of the Al-O symmetric stretching mode has a small departure from zero because the hydrogen atoms reduce the overall symmetry. In addition the hydrogen bonds to water also reduce its symmetry [17].

$Al_2O(OH)_6^{2-}$ species: A dimeric species, $Al_2O(OH)_6^{2-}$ is apparently formed by condensation of $Al(OH)_4^-$. Single crystal X-ray diffraction studies of the structure of solid potassium aluminate from precipitation of potassium aluminate solutions demonstrated the presence of discrete $Al_2O(OH)_6^{2-}$ anions built up from two AlO_4 tetrahedra which share an oxygen with the bridge AlOAl angle 132°[15]. The similarity of the Raman spectra of the solutions and the Raman and IR spectra of solid $Al_2O(OH)_6^{2-}$[10] and the fact that there was no detectable change in chemical shift from $Al(OH)_4^-$ in the ^{27}Al-NMR spectrum[6] all indicate the presence of $Al_2O(OH)_6^-$ with this structure.

Our Raman spectra for higher concentration solutions are comparable to those from R. J. Moolenaar et al.[10] and confirm the existence of $Al_2O(OH)_6^{2-}$ species. In Fig.4.1 and 4.2, besides the Raman bands of the $Al(OH)_4^-$ species, a

prominent Raman band at ~540 cm^{-1} is assigned to one AlOAl symmetric stretching mode and the bands at ~ 660 cm^{-1} are assigned to the four AlO_3 modes (Table 4.3). The additional bands of the $Al_2O(OH)_6^{2-}$ species, which were observed in the solid phase spectra[10], are very weak and may be overlapped by the bands of $Al(OH)_4^-$ near 320 and 620 cm^{-1}. The Raman spectra of solid $K_2Al_2O(OH)_6$ will be discussed later.

$Al(OH)_6^{3-}$ species: Two groups have proposed that the species $Al(OH)_6^{3-}$ may exist at low concentrations in highly caustic sodium aluminate solutions. This conclusion is based on a new Raman band at 470 cm^{-1}[11,12] and a very weak NMR resonance line at 0 ppm[9] observed in these solutions.

Our Raman studies reveal no Raman band at 470 cm^{-1} in solutions from low to high aluminium concentrations and high caustic ratios (Fig.4.1 and 4.2), even in those solutions stored in plastic bottles for more than three months. However, we noted that if the quartz tube was not pretreated with strong hydroxide, a weak Raman band could appear at around 460 cm^{-1}. This is apparently because considerable amounts of quartz dissolve into such high caustic solutions to form aluminosilicate complexes, as indicated by the irregular pits on the tube surface.

In the ^{27}Al NMR study, J.W. Akitt et al. observed a strong resonance line at 70 ppm with a very weak signal at 0 ppm in caustic sodium aluminate solutions at 45°C[9], although the

questions remains as to what species the strong signal at 70 ppm may be attributed. They proposed tentatively that $Al(OH)_4^-$ species exists in the solution. As we know, the chemical shift of $Al(OH)_4^-$ is always near 80 ppm. in the solution ^{27}Al NMR and is unaffected by the nature of the counter cation or by dilution[10]. In both solution and solid-state high-resolution ^{27}Al NMR, the range of the ^{27}Al NMR shifts for four-coordinated aluminium, is from 55 ppm in aluminosilicates up to 80 ppm in aluminates[50-52]. The ^{27}Al NMR line at about 70 ppm for the aluminosilicate species in aqueous solutions is linked to Al coordinated to two silicate centres[52,53]. Thus we can not exclude the possibility that the highly caustic sodium aluminate solution was contaminated by dissolution of the NMR quartz tube. If so the 70 ppm signal may arise from the aluminosilicate species. The source of the very weak resonance line at 0 ppm is unclear.

From the evidence presented here we confirm that two anionic species, i.e. $Al(OH)_4^-$ and $Al_2O(OH)_6^{2-}$ exist in the aqueous sodium aluminate solutions. There is no evidence to support the existence of the $Al(OH)_6^{3-}$ anion.

4.3.2. Induction process and precipitate products

Induction process: It is well known that supersaturated aluminate solutions will stay clear for a period of time before the nucleation and growth of a precipitate take place.

Our supersaturated sodium aluminate solutions remained clear for periods of a few days to over one month at room temperature.

The Raman spectra of sodium aluminate solutions were measured during this induction period. As examples, Figs. 4.3a and b show the Raman spectra of the solutions No.11 and 14 measured at time of < 1 hour and > 80 hours respectively after solution preparation, and normalized to the N-O stretching band of 0.23 M $NaNO_3$ as an internal standard. No spectral change over time was detected (Fig.4.3c). However, we found from our Raman measurements that the spectral baseline became more noisy with longer storage, indicating scattering light from colloidal particles. The intensity of the Raman band at ~540 cm^{-1} decreased rapidly in comparison with the intensity of the band at ~620 cm^{-1} once the precipitate appeared in the solutions.

Quantum calculations by the *ab initio* method[12] have shown that the Al-O bonds of $Al(OH)_4^-$ and $Al_2O(OH)_6^{2-}$ anions have a significant covalent character. Quantum calculations of excitation energy by the DV X_α method[12] also predict that the absorption frequencies of $Al(OH)_4^-$ and $Al_2O(OH)_6^{2-}$ are at about 230.0 and 266.6 nm respectively, and later has been detected by UV spectra at 270.0 nm[12].

From the combination of our Raman results with quantum calculations, it seems that both species, $Al(OH)_4^-$ and $Al_2O(OH)_6^{2-}$ anions are formed rapidly, with the latter forming

at the expense of the former, when $Al(OH)_3$ is dissolved in the concentrated NaOH solutions, and the concentrations of these two species remain constant in the induction period due to the slowness of mutual conversion of aluminate species which is caused by high activation energies of Al-O bond formation or breakage. After the induction period the clusters or colloids are formed with consumption of the less stable species, $Al_2O(OH)_6^{2-}$. When the clusters or colloids become big enough, the visible precipitate will be formed in the solutions.

Precipitate products: The precipitate produced from supersaturated potassium aluminate solutions has been proven to contain the $Al_2O(OH)_6^{2-}$ anion by X-ray diffraction, Raman and IR spectroscopes[10,15]. This result was also confirmed by our Raman spectra in Figs.4.4a and 4.5a. Our Raman spectrum showed a strong AlOAl symmetric stretching mode at 546.5 cm^{-1}, two AlO_3 stretching modes at 694 and 723 cm^{-1}, an OH bending mode at 902.5 cm^{-1}, the bending modes of the $O_3AlOAlO_3$ skeleton below 400 cm^{-1} and OH stretching modes over 3200 cm^{-1}. Table 4.4 summarizes the peak maxima for the solids and their assignments based on C_s symmetry for the $O_3AlOAlO_3$ skeleton[54].

The Raman spectra of precipitates from supersaturated sodium aluminate solutions are shown in Figs.4.4b and 4.5b. The spectra are mainly characterized by a strong band at 443

cm^{-1} along with a relatively strong band at 660.5 cm^{-1}. All Raman bands are listed in Table 4.5. There is no doubt that neither the $Al(OH)_4^-$ anion nor the $Al_2O(OH)_6^{2-}$ anion is present in this precipitate. When compared with Raman spectra of aluminum hydroxide polymorphs etc[55,56], it was determined that the precipitate was also not gibbsite, bayerite, nordstrandite, doyleite or boehmite. Because there are many crystalline forms of aluminum oxide and hydroxide and their structure are exceedly complex[57] the composition and structure for this precipitate is still not very clear from our Raman results.

As we know, the anionic species in aluminate solutions are the same regardless of the cation, but the precipitates are different. In the potassium aluminate solutions, after an induction period from preparation, the $Al_2O(OH)_6^{2-}$ anions are slowly crystallized out from the solution and form the crystal $K_2Al_2O(OH)_6$. However, in the sodium aluminate solutions, the precipitate produced does not contain the $Al_2O(OH)_6^{2-}$ species.

4.3.3. J values, formation quotients Q and equilibrium constant K

The above studies have shown that there are two anionic aluminate species, i.e. $Al(OH)_4^-$ and $Al_2O(OH)_6^{2-}$, in sodium aluminate solutions and that both species remain at constant

concentrations during the induction period. Therefore detailed quantitative Raman intensity studies using an internal standard can be used to elucidate the equilibria of sodium aluminate solutions.

The Raman spectra observed in the region 300-1200cm^{-1} for the solutions No.1 to No.16 are shown in Figs.4.1 and 4.2. The most prominent Raman bands are those corresponding to the Al-O symmetric stretching modes for the monomer, $Al(OH)_4^-$ and dimer, $Al_2O(OH)_6^{2-}$ with their maxima at ~620 and ~540 cm^{-1} respectively. The Al-O symmetric stretching modes at ~540 and ~620 cm^{-1} have higher Raman scattering intensities relative to the other vibrational modes and are less complicated by overlapping bands; therefore they can be used to obtain quantitative information. All spectra were carefully analyzed by curvefitting in the region containing the Al-O bands as exemplified in Fig.4.6. The band maxima (ν), halfwidths (hw) and areas (A_i), which were normalized by the 0.23 M NO_3^- ionic mode at 1052 cm^{-1} with 6000 area units, determined for the Al-O symmetric stretching modes at ~540 and ~620 cm^{-1} from the curvefit are listed in Table 4.6.

Calculation of J_i values: The Raman band areas A_i of the Al-O symmetric stretching modes at ~540 and ~620 cm^{-1} were assumed to be proportional to the concentration C_i of the corresponding species, i.e. $A_i = C_i * J_i'$ where J_i' is the molar scattering constant on a relative scale as Raman band areas A_i. In order to calculate the concentrations of the

$Al(OH)_4^-$ and $Al_2O(OH)_6^{2-}$ species from the measured Raman data, the molar scattering constants J_m' for the monomer, $Al(OH)_4^-$ and J_d' for the dimer, $Al_2O(OH)_6^{2-}$ must be known.

To obtain the J_m' value for the $Al(OH)_4^-$ species, the Raman spectra of the solutions No.1 - No.7 with a 1:4.1~4.4 mole ratio of $Al(OH)_3$(aq.) to Na(OH)(aq.) and an almost constant amount of sodium nitrate were recorded from 300 to 1200 cm^{-1}. As shown in Fig.4.1 and Table 4.6, the Raman band area A_d of the Al-O symmetric stretching mode at ~540 cm^{-1} for the $Al_2O(OH)_6^{2-}$ species in these solutions is dramatically decreased with the decreasing the concentration of aluminum and caustic ratio. In the solutions with low concentrations of aluminum and low caustic ratios, e.g. the solution No.1, only the Raman band area A_m of the Al-O symmetric stretching mode at ~620 cm^{-1} for the $Al(OH)_4^-$ species is easily observable. Therefore the J_m' value for the $Al(OH)_4^-$ species may be determined from such a solution when the total aluminum concentration approach zero.

The plot of total Raman band area A_t, i.e. A_m+A_d, for the Al-O symmetric stretching modes at ~540 and ~620 cm^{-1} vs total aluminum concentration C_t from chemical analyses given in Fig.4.7. The best fit for these data is: $A_t = 6589.0*C_t(T) + 709.1*C_t(T)^2 - 139.5*C_t(T)^3$. So that

$$J_m' = \lim_{C_t(T)\to 0} \frac{A_t}{C_t(T)} = 6.59(\pm 0.60)\cdot 10^3 \qquad (4.1)$$

The standard J_m value which is referred to the 1.0 M NO_3^- ionic mode at 1052 cm^{-1} with 1.0 area unit is 0.25±0.03.

To obtain the J_d' value for the $Al_2O(OH)_6^{2-}$ species, the Raman spectra for the solutions No.1 - No.15 were used for calculation. In the solutions No.1 to No.15, the total aluminum concentration C_t can be estimated as following:

$$C_t = C_m + 2 * C_d = \frac{A_m}{J_m'} + \frac{2 * A_d}{J_d'} \qquad (4.2)$$

Where the subscripts m and d mean the monomer, $Al(OH)_4^-$, and the dimer, $Al_2O(OH)_6^{2-}$. Using the estimated J_d' value, the known J_m' value and the Raman band areas A_i of the Al-O symmetric stretching modes at ~540 and ~620 cm^{-1} in Table 4.6, Eq.4.2 calculate a new $C_t(R)$ and performs a nonlinear least squares refinement of the J_d' to minimize the sum of the squares of the differences between the calculated results $C_t(R)$ and the chemical analyses $C_t(T)$ for the solutions No.1 - No.15. Calculated $C_t(R)$ values are shown in Table 4.7. With less than ± 10% standard deviation in the total concentration of aluminum between calculated results $C_t(R)$ and chemical analyses $C_t(T)$ (Table 4.7), the J_d' value obtained from the program SIGMA PLOT[49] is $1.48(\pm 0.48) * 10^4$ for the $Al_2O(OH)_6^{2-}$ species. Therefore the standard J_d value which is referred to the 1.0 M NO_3^- ionic mode at 1052 cm^{-1} with 1.0 area unit is 0.57(±0.18) for the $Al_2O(OH)_6^{2-}$ species.

Low concentration equilibria: With the known J_1' values, the concentrations of the $Al(OH)_4^-$ and $Al_2O(OH)_6^{2-}$ species for the solutions No.1 - No.7 may be calculated from the Raman band areas A_i (Table 4.6) of the Al-O symmetric stretching modes at ~620 and ~540 cm^{-1} respectively. The calculated results are listed in Table 4.7. The formation quotient Q for each solution may also be estimated according to the chemical formation equation:

$$2Al(OH)_4^- \rightleftharpoons Al_2O(OH)_6^{2-} + H_2O$$

and

$$Q = \frac{[Al_2O(OH)_6^{2-}]}{[Al(OH)_4^-]^2} = \frac{C_t(T) - [Al(OH)_4^-]}{2 \cdot [Al(OH)_4^-]^2} = \frac{C_t(T) - C_m(R)}{2 \cdot C_m(R)} \qquad (4.3)$$

The calculated log Q values are listed in Table 4.7. Here the total aluminum concentration $C_t(T)$ from chemical analyses and the $Al(OH)_4^-$ concentration $C_m(R)$ from Raman results are used in all calculations.

In the solutions No.1 -No.7, the formation quotients Q are different from the equilibrium constant K due to the significant change of water activity and ionic strength. However, from the above chemical formation equation, we know:

$$\log K = \log \frac{a_d \cdot a_{H_2O}}{a_m^2} = \log Q + \log \frac{\gamma_d}{\gamma_m^2} a_{H_2O} \qquad (4.4)$$

where $a_{m,d,H2O}$ and $\gamma_{m,d}$ are the activities and activity coefficients of the monomer $Al(OH)_4^-$, the dimer $Al_2O(OH)_6^{2-}$ and water.

Considering the Debye-Hückel theory of activity coefficients, the Eq.4.4 may be rewritten as:

$$\log Q = \log K + A \cdot I^{1/2} + B \cdot I + C \cdot I^{3/2} + \ldots\ldots \qquad (4.5)$$

where A = 1.018 at 298 K, which is the Debye-Hückel limiting slope, i.e. $\log\gamma = -0.509 * Z^2 * I^{1/2}$.

The plot of log Q vs $I^{1/2}$ for the solutions No.1 - 7 is shown in Figure 4.8 (rectangle). It is easily seen that the Q values decrease with decreasing ionic strength. The best fit for these data is:

$$\log Q = -2.552 + 1.018 \cdot I^{1/2} - 0.234 \cdot I + 0.029 \cdot I^{3/2} \qquad (4.6)$$

Extrapolation to zero ionic strength yields log Q = -2.55(±0.25) where the formation quotient is, by definition, the equilibrium constant K.

High concentration equilibria: The Raman spectra of the solutions No.8 to No.16 with pH around 15 and ionic strength

from 13 to 21 are shown in Fig.4.2. Table 4.6 lists the Raman band areas A_i of the Al-O symmetric stretching modes at ~540 and ~620 cm^{-1}. The calculated concentrations of the $Al(OH)_4^-$ and $Al_2O(OH)_6^{2-}$ species from the Raman data are given in Table 4.7. With the total aluminum concentration $C_t(T)$ from chemical analyses and the $Al(OH)_4^-$ concentration $C_m(T)$ from the Raman data, the formation quotients Q were determined by Eq.4.3 and listed in Table 4.7.

The formation quotient log Q vs ionic strength $I^{1/2}$ for the solutions No.8 to No.16 is plotted in Fig.4.8 (circle). It is easily seen that the Q value decreases with decreasing ionic strength. All data show that log Q varies with I, i.e. Eq.4.6 is a good model.

The above quantitative Raman studies show that the distribution of $Al(OH)_4^-$ and $Al_2O(OH)_6^{2-}$ species depends strongly on the ionic strength and its effect on activity coefficients and the activity of water. The $Al_2O(OH)_6^{2-}$ species is much more stable in highly caustic solutions than low alkalinity solutions for these reasons.

In addition, an interesting observation made here was that the $Al(OH)_4^-$ species only has a little increase in concentration at temperatures up to 150°C by consuming the $Al_2O(OH)_6^{2-}$ species. The results are presented in Chapter 5.

Table 4.1. Solution Compositions Investigated in This Work

No.	Al^{3+}	Na^+	OH^- †	NO_3^-
-- Solutions for equilibria studies at $Al(OH)_3$/NaOH ratios of 1:4.1~4.4				
1	0.56	2.59	4.04	0.23
2	0.84	3.83	6.12	0.23
3	1.12	4.75	7.88	0.23
4	1.62	7.23	11.86	0.23
5	2.08	9.24	15.25	0.23
6	3.23	13.25	22.71	0.23
7	4.16	17.24	29.49	0.23
--Solutions for equilibria studies at higher hydroxide concentrations				
8	1.03	13.54	16.40	0.23
9	1.42	12.77	16.80	0.23
10	1.85	12.63	17.95	0.23
11	1.99	15.99	21.73	0.23
12	2.39	16.90	23.84	0.23
13	3.03	18.02	26.88	0.23
14	3.54	19.37	29.76	0.23
15	4.07	17.59	29.57	0.23
16‡	4.16	17.24	29.49	0.23

† $[OH^-]$ is the sum of all hydroxide concentrations from $Al(OH)_3$ and NaOH. All solution concentrations are in mol/liter.

‡ No.16 = No.7.

Table 4.2. Raman Data for Sodium Aluminate Solutions No.1 and No.7

Solution No.1		Solution No.7	
~ 325	w, dp†	~ 325	w, dp
~ 540	vw, p	538	s, p
619.5	s, p	621.5	s, p
-		661.5	w, p
710.5	w, dp	710.5	w, dp

† vw: very weak; w: weak; m: middle; s: strong; p: polarized; dp: depolarized.

All band maxima are in cm^{-1}.

Table 4.3. Assignments of Raman Bands for the $Al(OH)_4^-$ and $Al_2O(OH)_6^{2-}$ Species

Raman (cm^{-1})	Assignments
----- $Al(OH)_4^-$ species	
~325 w, dp	AlO_4 antisymmetric bending ($\nu_{2,4}$)
620 s, p	AlO_4 symmetric stretching (ν_1)
710 w, dp	AlO_4 antisymmetric stretching (ν_3)
----- $Al_2O(OH)_6^{2-}$ species	
540 s, p	AlOAl symmetric stretching
660 w, dp	AlO_3 stretching modes

Table 4.4. Vibrational Spectra and Assignment for $[(OH)_3AlOAl(OH)_3]^{2-}$

IR†(cm^{-1})	Raman‡(cm^{-1})	Assignments[#]
	3587.5 m	O-H stretch (Free OH)
3540 m	3497 mw	O'-H stretch
3370 m	3380 w	O"-H stretch
3275 m	3251.5 w	O"'-H stretch
1105 m		O"'-H bend
920 ms*		$\nu(AlO_3)$ A'(2)
870 mw	902.5 w	O"-H bend
725 s	723 mw	
700 s	694 w	$\nu(AlO_3)$(4) A' and A",
685 s		overlapping
628 m		O'-H bend
	630 w	$\nu_{antisymmetric}$ (AlOAl)A'
	592.5 w	?
545 m	546 s	$\nu_{symmetric}$ (AlOAl)A'
	445 vw	?
385 sh	391 w	
374 m		
344 m		Bending modes
325 m		of skeleton
270 m	281 mw	
226 w	234.5 w	

† IR data from reference 10. ‡ All Raman data from this work.

mw: middle weak; ms: middle strong; sh: shoulder.

Table 4.5. Raman Bands for the Precipitate from Sodium Aluminate Solutions

Raman (cm^{-1})		Raman (cm^{-1})	
3620	w	3463	vw
995	w	784.5	w
742	w	660.5	ms
608	w	582	w
500	w	443	s
399	w	361	vw
282	w	235	w

Table 4.6. The Raman Band Maxima (ν), Halfwidths (hw) and Areas (A_i) of Sodium Aluminate Solutions No.1 - No.16 at Room Temperature (25°C)

No.	ν_m(hw)	ν_d(hw)	A'_m	A_d	A_t ‡
1	619(28)	547(82)	3561.9	414.2	3976.1
2	619.5(28)	547(82)	4975.2	1041.9	6017.1
3	619.5(28)	547(82)	6342.6	1625.3	7967.9
4	619.5(28)	547(82)	8538.2	3175.1	11713.3
5	620(28)	541(82)	9420.3	6372.5	15792.8
6	621.5(26)	538.5(80.5)	10009.4	13889.3	23898.7
7(16)	621.5(26)	538(81)	9421.7	20237	29658.7
8	619.5(26)	543(80.5)	4310.2	3270.6	7580.8
9	620.5(26)	544(81)	5785.5	4721.3	10506.8
10	620.5(26)	542.5(80)	6675.6	7167.8	13843.4
11	621.5(26)	540.5(80)	7060.7	7886.4	14947.1
12	621.5(26)	540.5(80)	6582.4	10263	16845.4
13	621.5(26)	538.5(80.5)	7027.2	13485	20512.2
14	621.5(26)	538.5(81)	7852	16587	24439
15	621.5(26)	538.5(80)	8475	19305	27780

† All areas (A_i) are normalized to the 0.23 M NO_3 ionic mode at 1052 cm^{-1} with an area of 6000 units. Raman band maxima and halfwidths are in cm^{-1}. A_m and A_d are the Raman band areas for the Al-O symmetric stretching modes at ~620 and 540 cm^{-1} respectively.

‡ $A_t = A_m + A_d$

Table 4.7. The Calculated Results for the Solutions No.1 - No.16 from Raman Data and Chemical Analys

No.	$C_t(T)$†	$C_m(R)$†	$2*C_d(R)$	$C_t(R)$‡	e%@	log Q	$I^{1/2}$
1	0.56	0.54	0.06	0.60	7.14	-1.465	1.61
2	0.84	0.76	0.14	0.90	7.14	-1.160	1.97
3	1.12	0.96	0.22	1.18	5.36	-1.062	2.20
4	1.62	1.29	0.43	1.72	6.17	-1.004	2.72
5	2.08	1.43	0.86	2.29	10.1	-0.799	3.09
6	3.23	1.52	1.88	3.40	5.26	-0.432	3.76
7 (16)	4.16	1.43	2.74	4.17	0.24	-0.176	4.31
8	1.03	0.65	0.44	1.09	5.83	-0.347	3.71
9	1.42	0.88	0.64	1.52	7.04	-0.458	3.61
10	1.85	1.01	0.97	1.98	7.02	-0.385	3.62
11	1.99	1.07	1.07	2.14	7.54	-0.396	4.06
12	2.39	1.00	1.39	2.39	0.00	-0.158	4.19
13	3.03	1.07	1.82	2.89	-4.62	-0.068	4.36
14	3.54	1.19	2.24	3.43	-3.11	-0.081	4.53
15	4.07	1.29	2.61	3.90	-4.18	-0.078	4.35

† The aluminum concentrations (moles per litre) are from Chemical (Titration) and calculated (Raman) methods.

‡ $C_t(R) = C_m(R) + 2*C_d(R)$

@ *Percentage*, $e\% = \frac{C_t(R) - C_t(T)}{C_t(T)}\%$

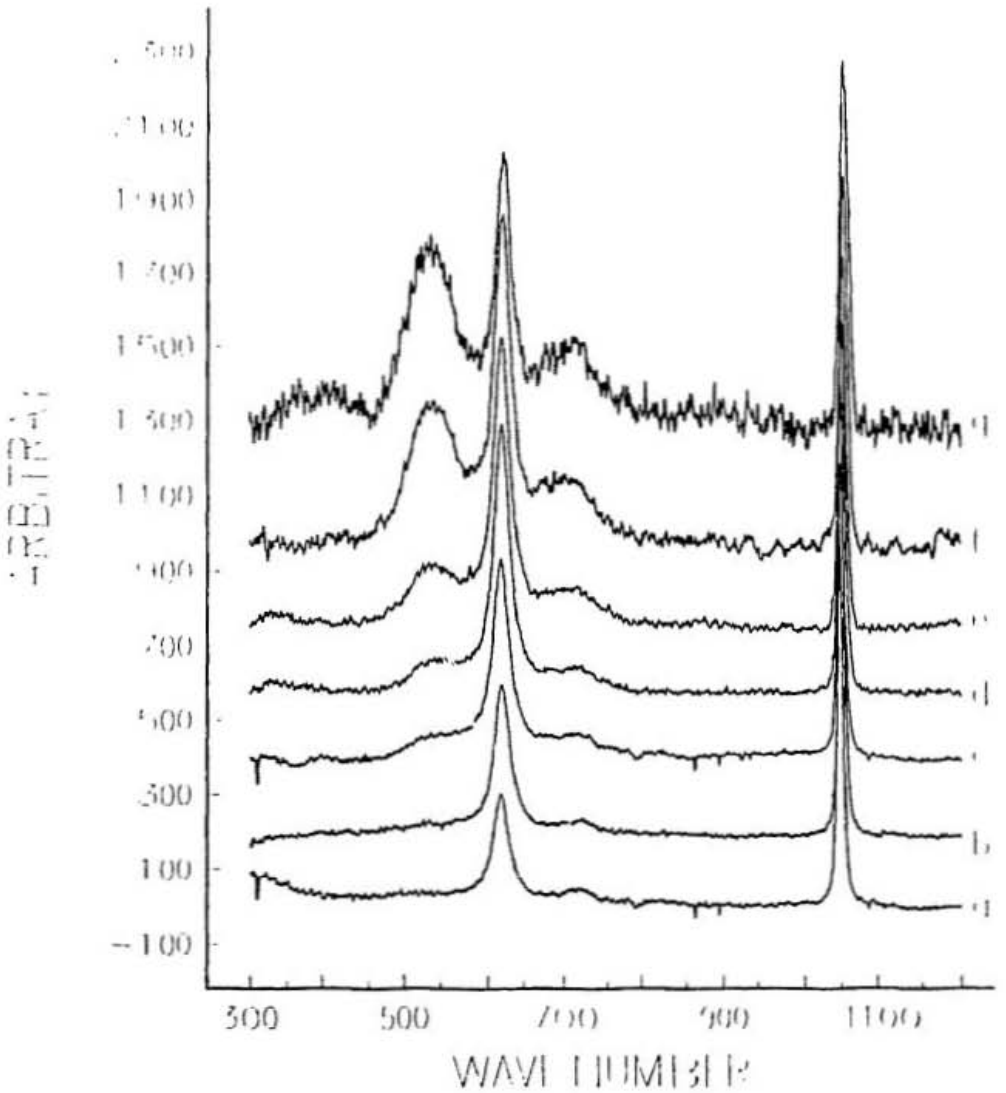

Figure 4.1. Raman Spectra (300-1200 cm^{-1}) of Solutions (a) No.1, $[Al^{3+}]$=0.56M; (b) No.2, $[Al^{3+}]$=0.84M; (c) No.3, $[Al^{3+}]$=1.12M; (d) No.4, $[Al^{3+}]$=1.62M; (e) No.5, $[Al^{3+}]$=2.08M; (f) No.6, $[Al^{3+}]$=3.23M; and (g) No.7(16), $[Al^{3+}]$=4.16M at Room Temperature (25°C)

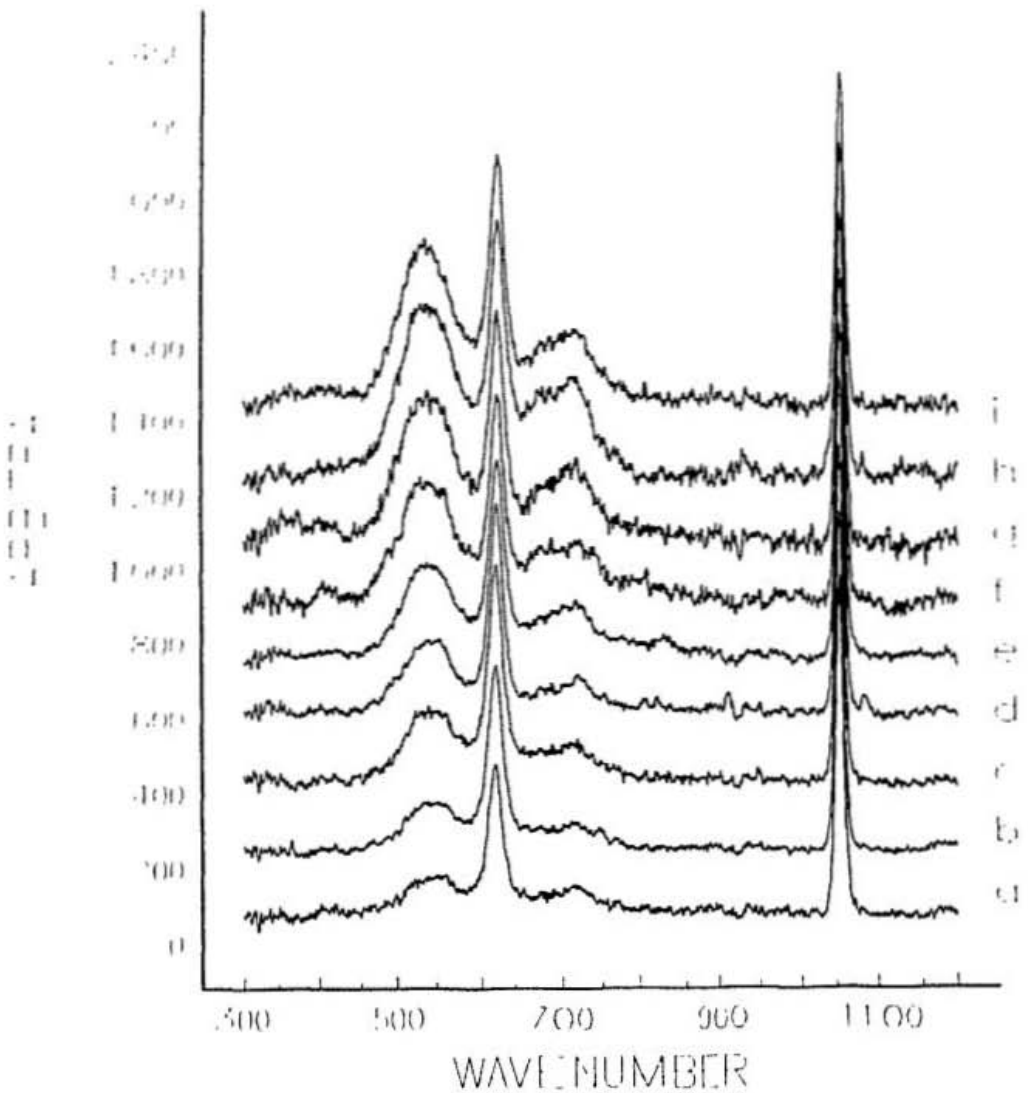

Figure 4.2. Raman Spectra (300-1200 cm^{-1}) of Solutions (a) No.8, $[Al^{3+}]$=1.03M; (b) No.9, $[Al^{3+}]$=1.42M; (c) No.10, $[Al^{3+}]$=1.85M; (d) No.11, $[Al^{3+}]$=1.99M; (e) No.12, $[Al^{3+}]$=2.39M; (f) No.13, $[Al^{3+}]$=3.03M; (g) No.14, $[Al^{3+}]$=3.54M; (h) No.15, $[Al^{3+}]$=4.07M and (i) No.16(7), $[Al^{3+}]$=4.16M at Room Temperature (25°C)

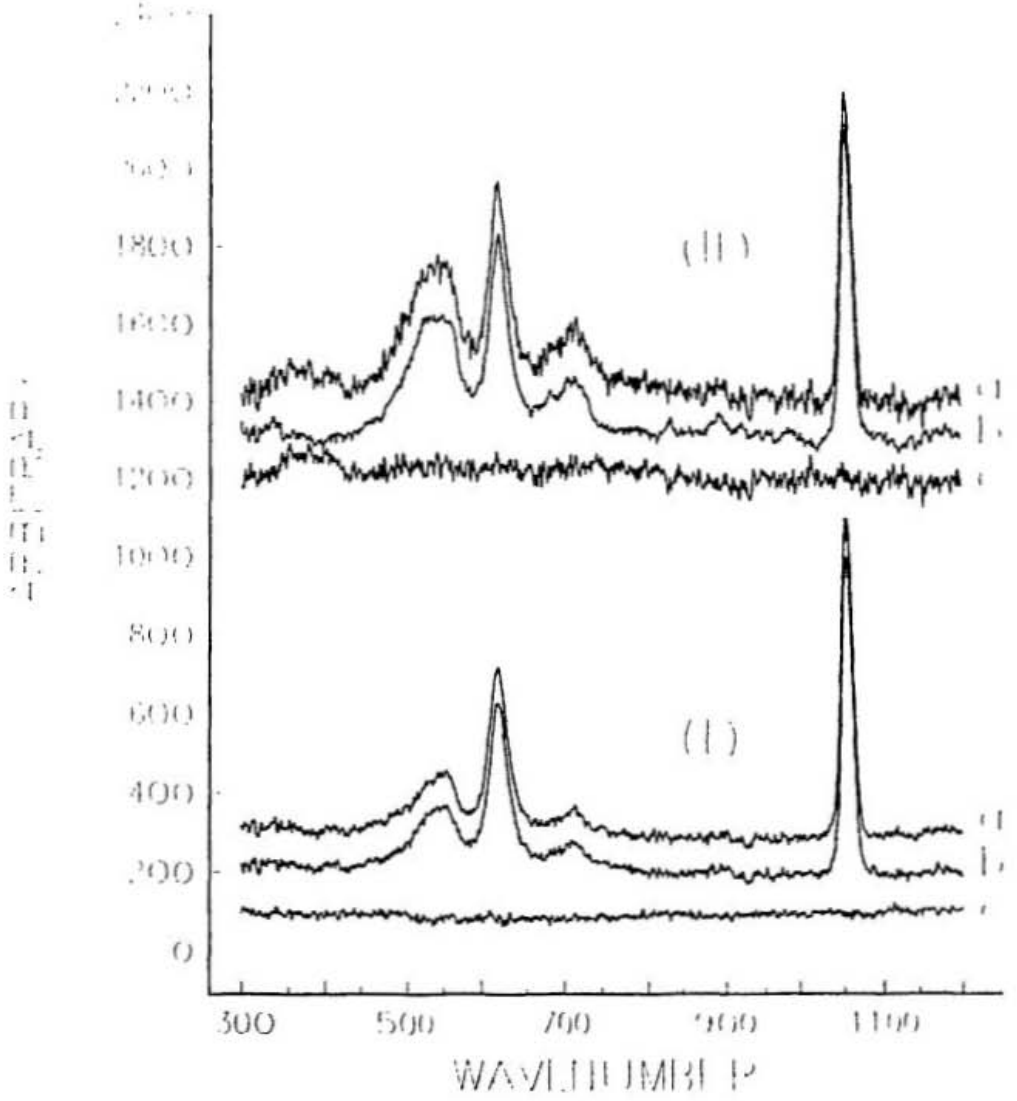

Figure 4.3. Raman Spectra (300-1200 cm^{-1}) of the Solutions (I) No.11 and (II) No.14 at Room Temperature (25°C); (a) t < 1 hour, (b) t > 80 hours and (c) a-b

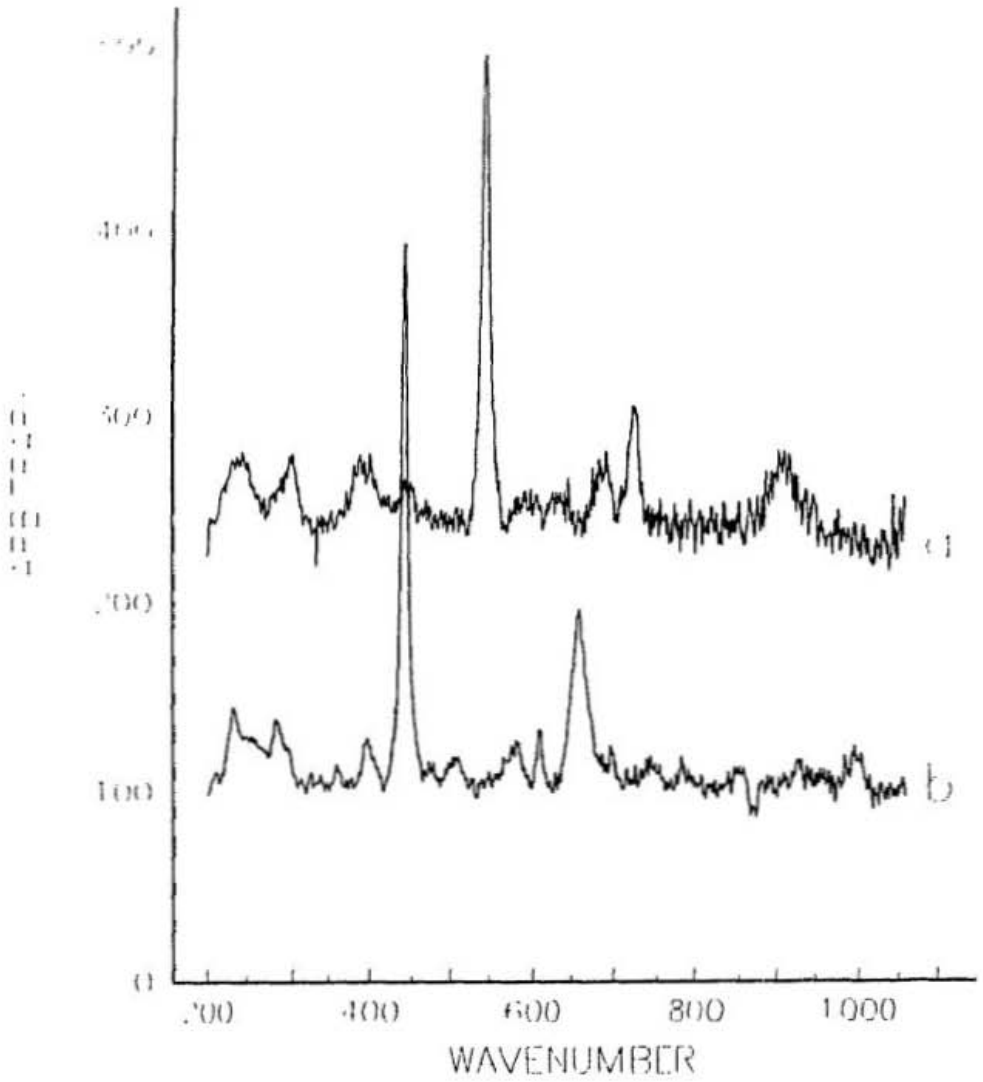

Figure 4.4. Raman Spectra (200-1000 cm^{-1}) of Precipitates from (a) the Potassium Aluminate Solutions and (b) the Sodium Aluminate Solutions

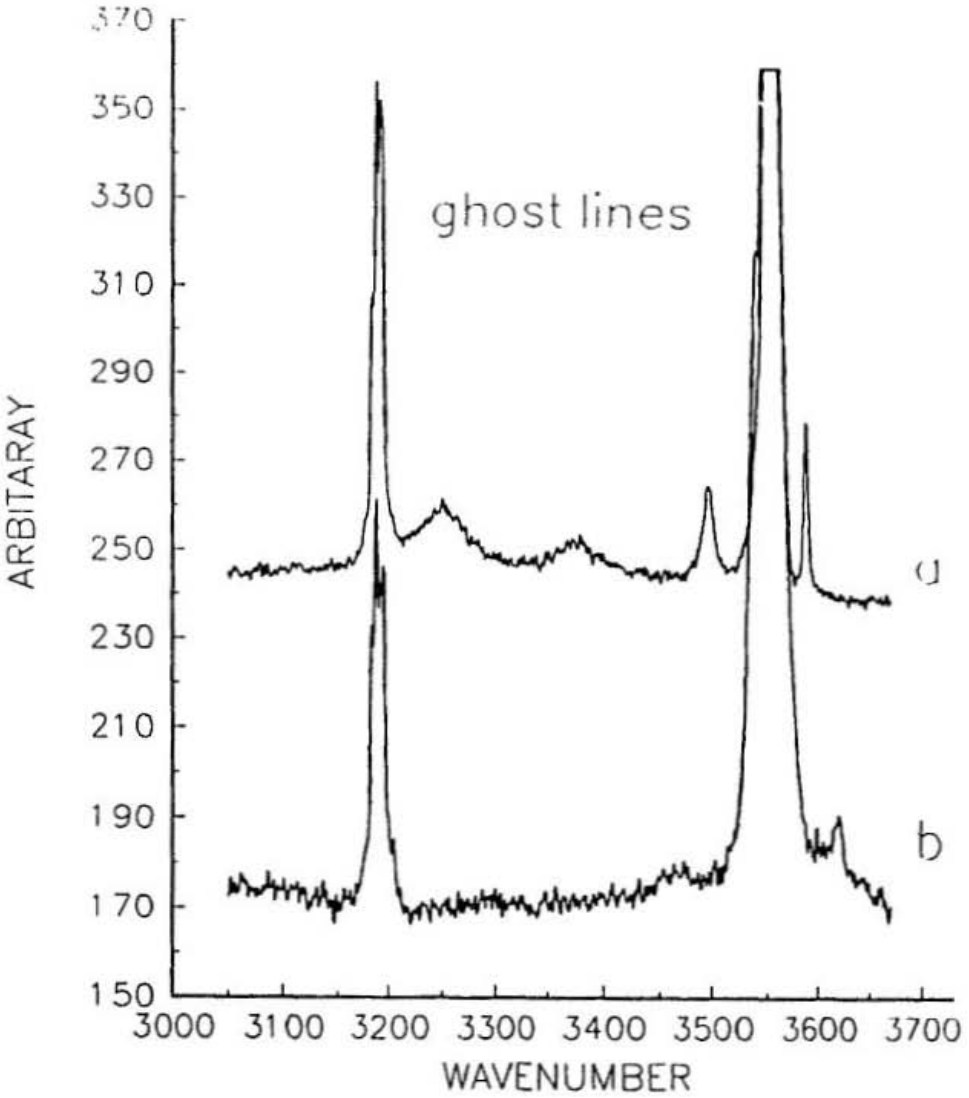

Figure 4.5. Raman Spectra (3000-3650 cm^{1}) of Precipitates from (a) the Potassium Aluminate Solutions and (b) the Sodium Aluminate Solutions

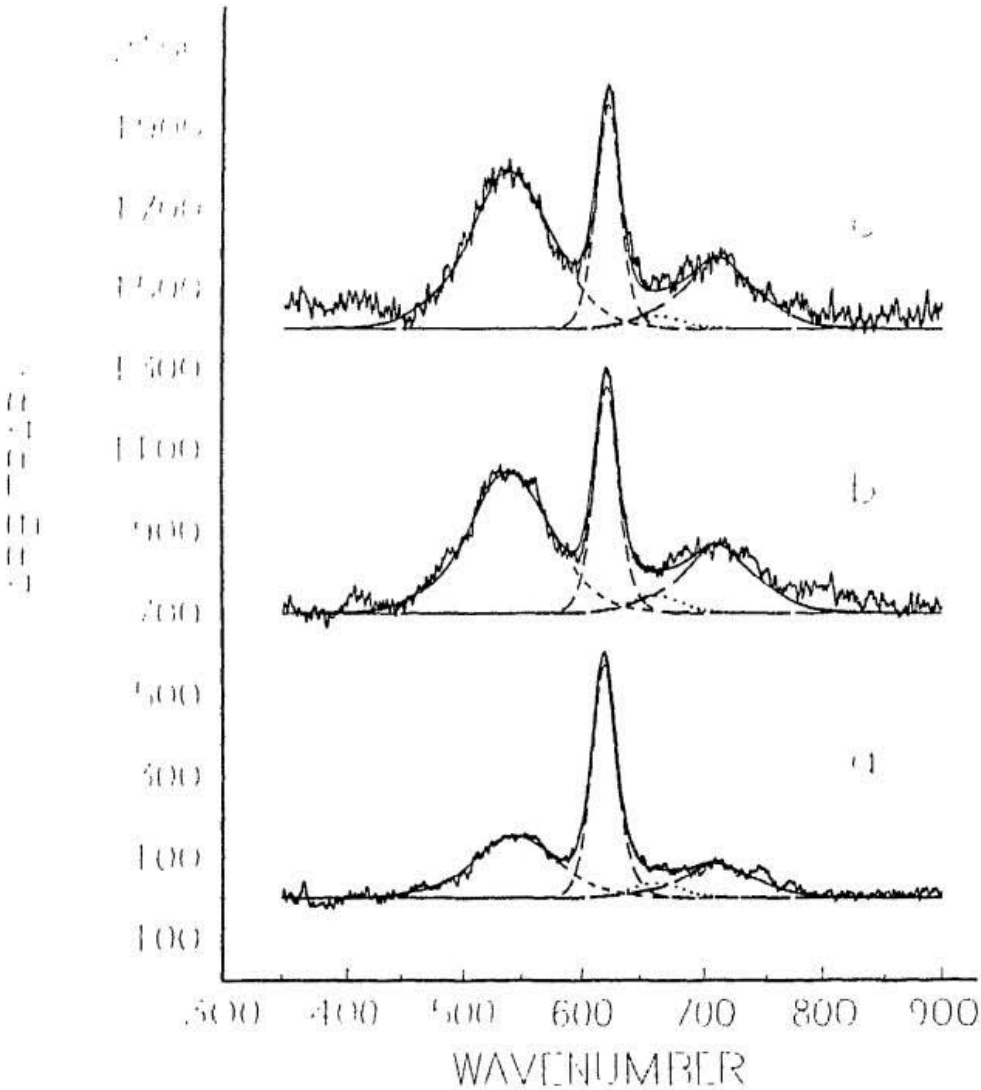

Figure 4.6. Examples of Curvefitting (350-900 cm^{-1}) for the Solutions (a) No.9, (b) No.13 and (c) No.15

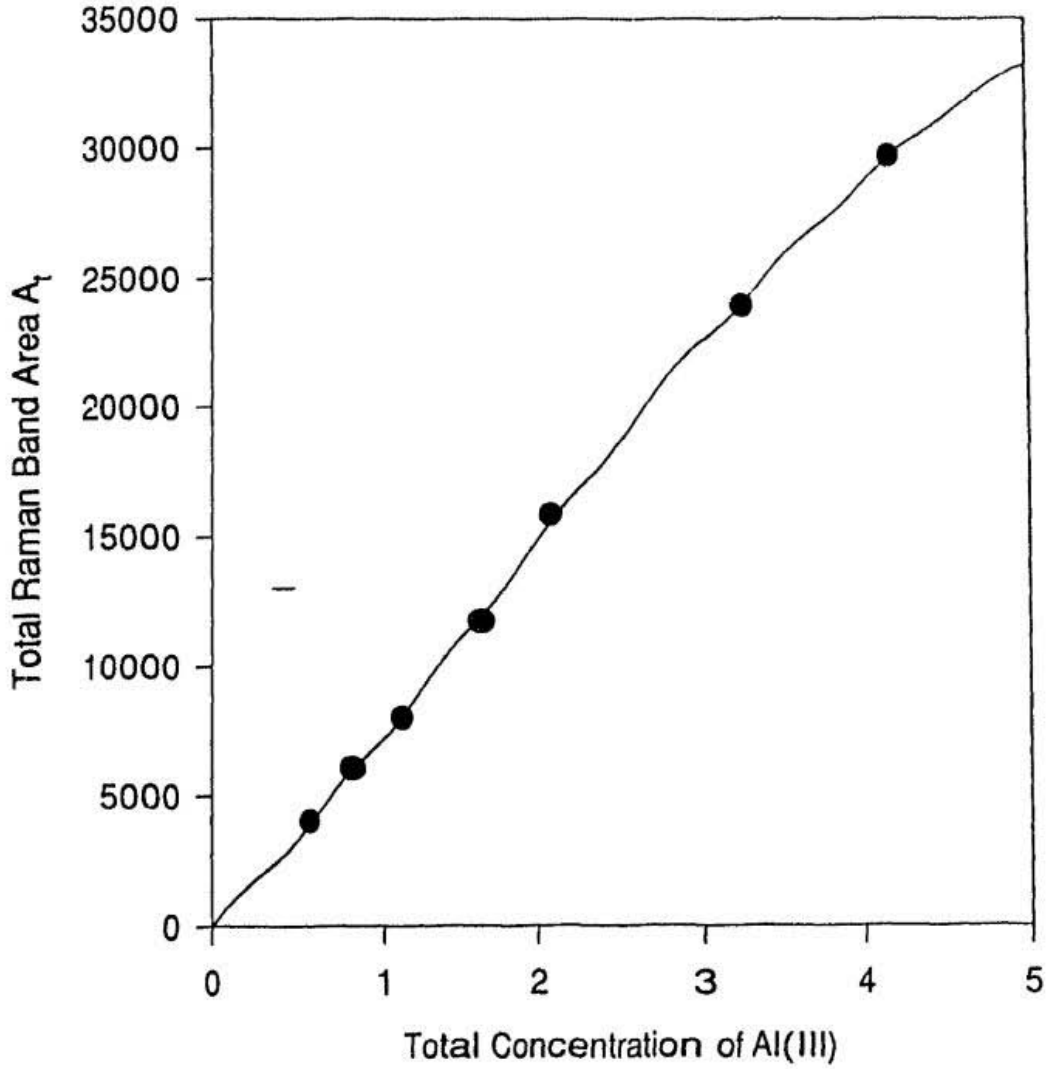

Figure 4.7. The Total Raman Band Areas A_t, i.e.(A_m+A_d), for Al-O Symmetric Stretching Modes at ~540 and ~620 cm^{-1} vs Total Aluminum Concentrations $C_t(T)$ from Chemical Analyses for the Solutions No.1 - No.7

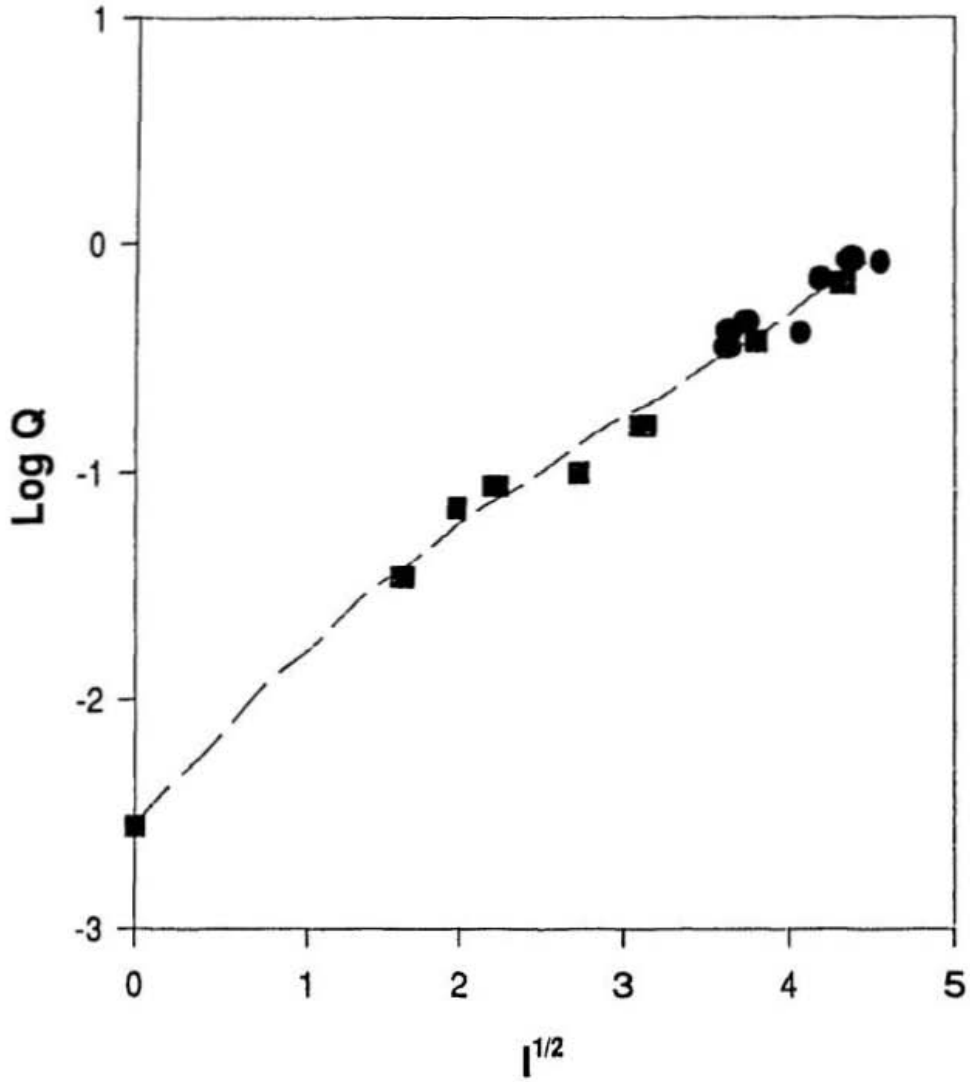

Figure 4.8. Formation Quotients log Q vs Ionic Strength $I^{1/2}$ for the Solutions No.1 - No.7 (Rectangle) and the Solutions No.8 - No.16 (Circle)

Chapter 5. Studies on Hydrogen Bonds to Carbonate and Aluminate Anions in Aqueous Solutions at Temperatures up to 150°C

5.1. Introduction

Hydrogen bonds play a very important role in the intermolecular structure of aqueous solutions. Hence studies on the hydrogen-bonding properties of aqueous solutions are obviously helpful for us to understand electrolyte hydration as well as bulk water.

Vibrational spectroscopy has been proved as an ideal technique to study electrolyte hydration in aqueous solutions. The information about electrolyte hydration may be directly obtained from the observation of new Raman bands in the low frequency region (200-500 cm^{-1}) or indirectly from the change in the Raman and IR spectra of hydrated water[1,4]. However the bands arising from electrolyte hydration are very weak. It is difficult to study temperature and concentration effects on electrolyte hydration by these bands.

Recently, the results of Raman studies of vibrational modes of aqueous carbonate, aluminate and other hydroxy complexes at room temperature have provided information about the hydrogen bonding of water to oxide and hydroxide groups

in these complexes[17,18].

In this chapter, we will report measurements of the differences in Raman band frequencies and halfwidths of carbonate and aluminate vibrational modes in H_2O and D_2O at 25°C and elevated temperatures. The results provide information about the temperature dependence of hydrogen bond interactions and the hydration of these important anionic species. It will be shown that hydrogen bonds are much less affected by increased temperature than previously believed[1-4].

5.2. Experiments and Results

Reagent grade K_2CO_3 and γ-$Al(OH)_3$ (gibbsite) were dried in an oven at ~110°C for two hours and then cooled in a vacuum desiccator over silica gel. Aqueous solutions of 5.0 M potassium carbonate were prepared by dissolving weighed K_2CO_3 in H_2O and D_2O. The sodium aluminate solution was prepared by dissolving weighed γ-$Al(OH)_3$ and NaOH in H_2O. The deuterated analogue of sodium aluminate solution was prepared by dissolving a weighed amount of aluminum metal into a solution of NaOD in D_2O. Two sodium aluminate solutions had ~1.0 M aluminium concentrations and a ~1:4.2 mole ratios of $Al(OH(D))_3(aq)$ to NaOH(D)(aq). All solutions were passed through an activated charcoal filter and then sealed in

quartz tubes, pre-treated with aqueous sodium hydroxide solution.

The Raman spectra were obtained with a Coderg PHO Raman spectrometer with sample excitation by the 488 nm line of an argon laser. The methods for recording and treating the Raman data have been described in Chapter 4.

Representative spectra for ~5.0 M aqueous CO_3^{2-} in H_2O and D_2O, ~1.0 M aqueous $Al(OH)_4^-$ in H_2O and its deuterated analogue in D_2O at temperatures up to 150°C are shown in Figs.5.1, 5.2, 5.3 and 5.4 for the in-plane bending mode (ν_4) region of the carbonate anion and the Al-O symmetric stretching mode (ν_1) region of the tetrahedral species. The frequencies and halfwidths are listed in Tables 5.1 and 5.2.

5.3. Discussion

5.3.1. Hydrogen bonds to carbonate anion

The infrared and Raman spectra of the aqueous carbonate anion have been interpreted in terms of a planar D_{3h} species slightly distorted by water solvation and, possibly cation-anion interactions[58]. Distortion is suggested because among the four fundamental vibration modes predicted by the D_{3h} point group, the Raman forbidden out-of-plane deformation mode (ν_2) at ~ 885 cm^{-1} and infrared forbidden symmetric stretching mode (ν_1) at ~1060 cm^{-1} were observed, and the

asymmetric stretching mode (ν_3) at around 1400 cm^{-1} was found to be resolved into two bands in both Raman and Infrared spectra. Recently, the significant differences in the frequencies and halfwidths of Raman spectra lines for the in-plane bending mode (ν_4) of aqueous carbonate in H_2O and D_2O were also observed at room temperature[18]. This new observation can be interpreted to provide information on the hydrogen bonding of water to carbonate and subtle differences between hydrogen and deuterium hydrogen bonding.

Raman spectra for the ν_4 mode of carbonate anion for 5.0 M aqueous K_2CO_3 in H_2O and D_2O are illustrated in Figs.5.1 and 5.2. At room temperature, in normal water, the peak maximum is at 683.5 cm^{-1} and the halfwidth is 38.5 cm^{-1}. In heavy water, the peak maximum is at 698.5 cm^{-1} and the halfwidth is 25 cm^{-1}. The peak maximum for the ν_4 mode is 15 cm^{-1} higher in D_2O than in H_2O. These results were found to be independent of temperature from 25°C to 150°C (Table 2), at concentrations from 1.0 to 6.0M[18]. Similar differences in peak maxima and halfwidths were also noted in other regions of the Infrared and Raman spectra (Table 5.1). Similar studies of aqueous nitrate[18], whose vibrational spectra were interpreted in terms of solvation and contact ion-pairing effects[59], revealed that the peak maxima were identical for nitrate salts dissolved in H_2O and D_2O although small differences in halfwidths were detected (Table 5.1).

These results provide compelling evidence for strong

hydrogen bonding interactions between water and carbonate at temperatures up to 150°C and quantify the difference between the strength of the hydrogen bond interactions for hydrogen and deuterium. In reality, all the vibrational modes of the hydrogen-bonded species are affected, to a greater or lesser extent, by substitution of normal water by heavy water. An explanation for the differences in Raman frequencies and halfwidths for the ν_4 mode of aqueous carbonate can be deduced from differences in zero point energies of H_2O and D_2O. Heavy water is considered to be more structured than normal water because the thermal amplitudes of vibration are smaller[60]. The contribution of bending modes is particularly important because the smaller displacements associated with bending modes in D_2O tend to favour stronger more linear hydrogen bonds for deuterated systems. In the present case the stronger hydrogen bonds of deuterated water to carbonate result in greater resistance to the bending motion of the ν_4 mode and a larger force constant. The decrease in the halfwidth for carbonate in D_2O can be attributed to a smaller distribution of environments in the more ordered deuterated water. In contrast the small differences between the vibrational spectrum of nitrate in H_2O and D_2O suggest weaker hydrogen bonding of water to nitrate.

5.3.2. Hydrogen bonds to aluminate anion

The anomalous frequency shifts and halfwidth differences in the Raman spectra of hydroxy complexes and their deuterated analogues have been used to measure the differences in the hydrogen bonding of water to the hydroxide ion of the hydroxy complexes[17]. In our Raman spectra of sodium aluminate solutions (Figs.5.3 and 5.4), we also find that the halfwidth of the ν_1 symmetric stretching mode of the $Al(OH)_4^-$ species at 619.5 cm^{-1} (26.5 cm^{-1}) is significantly smaller than that for the $Al(OD)_4^-$ species at 601 cm^{-1} (38 cm^{-1}) at room temperature. Increasing the temperature up to 150°C has no effect on the frequencies and halfwidths of these Raman spectra (Table 5.2).

Normally, the halfwidths of Raman bands will decrease when deuterium is substituted for hydrogen because the thermal amplitude of deuterium is less and therefore the range of the environments for deuterium sensitive modes of vibration will be less[60]. The anomalous halfwidth difference between the ν_1 symmetric stretching modes of the $Al(OH)_4^-$ and $Al(OD)_4^-$ species requires the need to invoke strong hydrogen bonds from the O of the hydroxide to the H of the hydrogen bonded water (Fig.5.5). The metal-oxygen vibrations of the complex will have a tendency to be pulled offline by the effects of hydrogen bonding. The deuterium samples will have a wider range of environments because the heavier mass of the deuterated water will tend to pull the oxygen even more offline and increase the range of environments.

As we know, under the Born-Öppenheimer approximation the force constant for each hydrogen-deuterium pair should remain constant. Therefore, the predicted frequency shift from theory should only be dependent on the square root of the mass ratio. Our measured frequency shift between the ν_1 symmetric stretching bands of the $Al(OH)_4^-$ and $Al(OD)_4^-$ species is slightly greater than the predicted value on the basis of a change in mass of 17 to 18 on substitution of OH by OD. The fact that the mass of the hydroxy anion appears to be too large can also be attributed to the effects of hydrogen bonding to water.

The Raman spectra of the ν_1 mode for aqueous $Al(OH)_4^-$ and $Al(OD)_4^-$ provide compelling evidence for the presence of strong hydrogen bonding of water in the outer hydration sphere to the oxygen of the hydroxy ligand in the first coordination sphere. This hydrogen bond has no significant change at temperature up to 150°C.

Table 5.1. The Infrared and Raman Band Maxima†(ν) and Halfwidths (hw) for Aqueous CO_3^{2-}, NO_3^-, $Al(OH)_4^-$ and $Al(OD)_4^-$ in H_2O and D_2O at Room Temperature (25°C)

		H_2O	D_2O
CO_3^{2-}	ν_1 (IR)	1060(16)	1059(16)
	$\nu_1(R_{iso})$‡	1063.6(11)	1062.2(11)
	$\nu_1(R_{aniso})$	1063.6(12)	1062.2(12)
	ν_2(IR)	884(26)	879(11)
	ν_4(R)	683.5(38.5)	698.5(25)
NO_3^-	ν_1(IR)	1047.7(19)	1047.7(19)
	$\nu_1(R_{iso})$	1052(12)	1052(12)
	$\nu_1(R_{aniso})$	1052(16)	1052(16)
	ν_2(IR)	828(10)	828(7)
	ν_4(R)	717.5(21.5)	717.0(16.0)
$Al(OH)_4^-$	ν_1(R)	619.5(26.5)	-
$Al(OD)_4^-$	ν_1(R)	-	601(38)

† The Raman band maxima and halfwidths are in cm^{-1}.

‡ $I_{iso} = I_{\parallel} - (4/3)*I_{\perp}$; $I_{aniso} = I_{\perp}$.

Table 5.2. The Raman Band Maxima (cm^{-1}) and Halfwidths (cm^{-1}) for ν_1 of Aqueous CO_3^{2-} and for ν_1 of Aqueous $Al(OH)_4^-$ and $Al(OD)_4^-$ in H_2O and D_2O at Temperature up to 150°C

T(°C)	CO_3^{2-}		$Al(OH)_4^-$	$Al(OD)_4^-$
	(H_2O)	(D_2O)	(H_2O)	(D_2O)
25	683.5(38.5)	698.5(25)	619.5(26.5)	601(38)
50	683(38)	698.5(25)	619.5(27)	601(38)
75	683.5(38.5)	698(25.5)	619.5(26.5)	600.5(38.5)
100	683.5(38.5)	698(25.5)	619.5(26.5)	600.5(38.5)
115	683.5(38)	698(25.5)	619.5(26.5)	601(38.5)
130	683.5(38)	698(26)	619.5(27)	600.5(38)
150	683(39)	698.5(25)	619.5(26)	600.5(39)

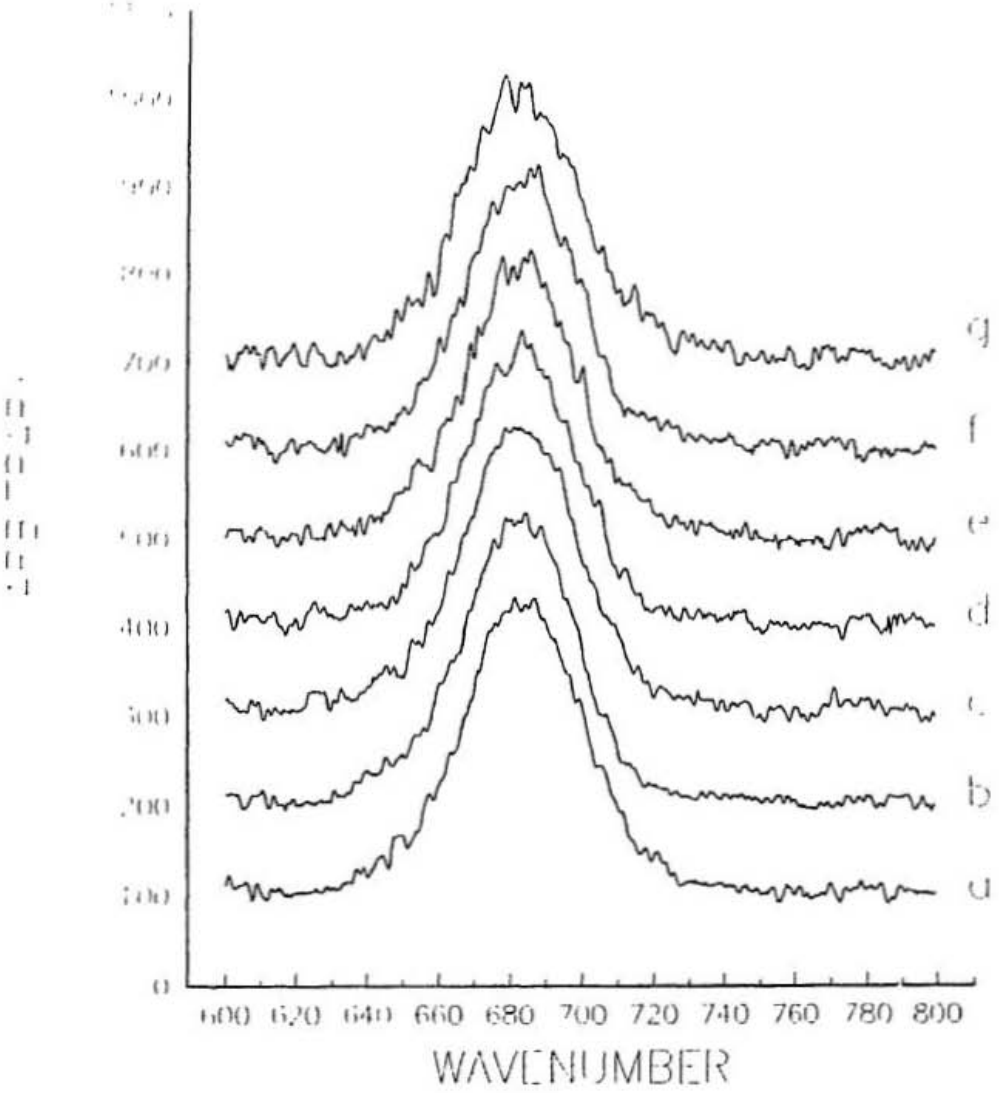

Figure 5.1. Raman Spectra (600-800 cm^{-1}) of CO_3^{2-} in H_2O at (a) 25°C, (b) 50°C, (c) 75°C, (d) 100°C, (e) 115°C, (f) 130°C and (g) 150°C

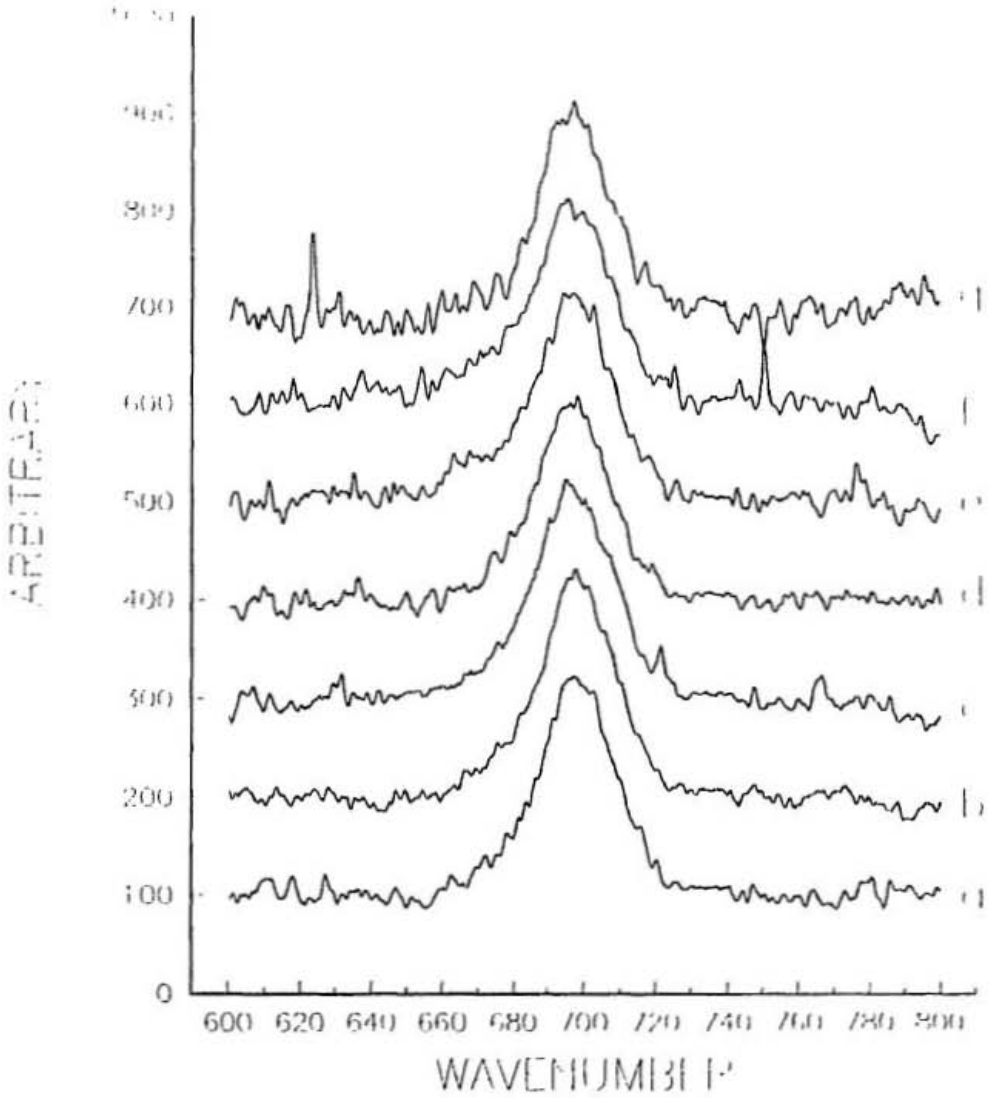

Figure 5.2. Raman Spectra (600-800 cm^{-1}) of CO_3^{2-} in D_2O at (a) 25°C, (b) 50°C, (c) 75°C, (d) 100°C, (e) 115°C, (f) 130°C and (g) 150°C

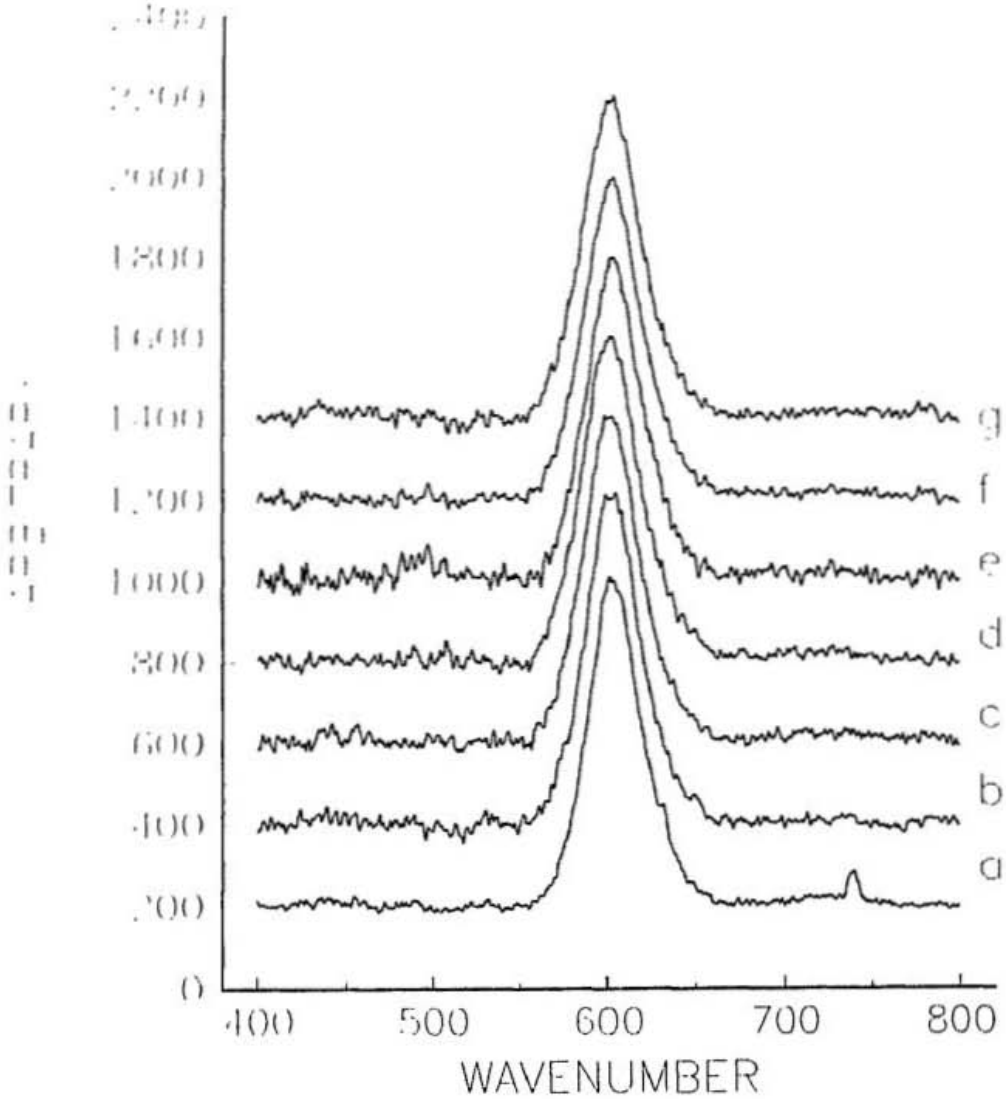

Figure 5.3. Raman Spectra (400-800 cm^{-1}) of $Al(OH)_4^-$ in H_2O at (a) 25°C, (b) 50°C, (c) 75°C, (d) 100°C, (e) 115°C, (f) 130°C and (g) 150°C

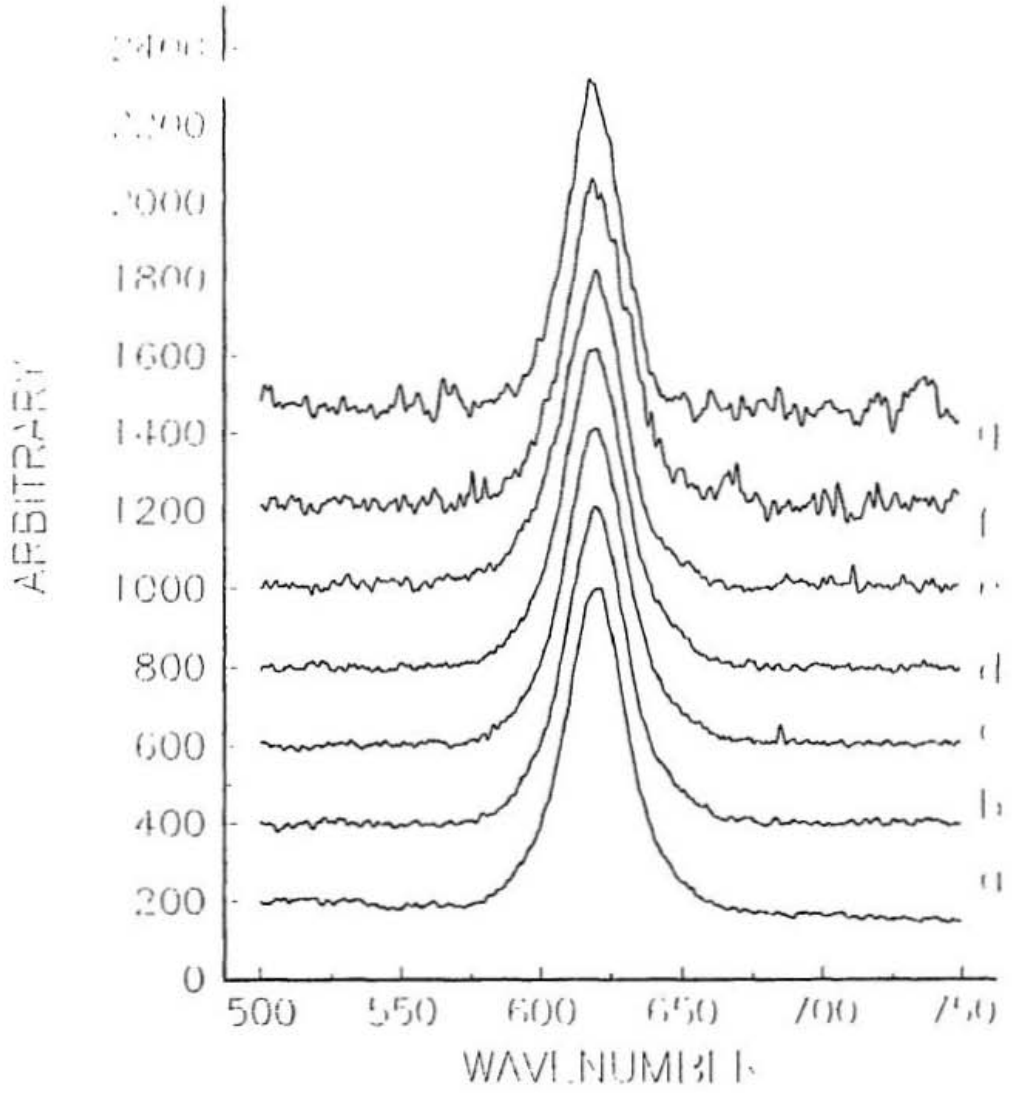

Figure 5.4. Raman Spectra (500-750 cm^{-1}) of $Al(OD)_4^-$ in D_2O at (a) 25°C, (b) 50°C, (c) 75°C, (d) 100°C, (e) 115°C, (f) 130°C and (g) 150°C

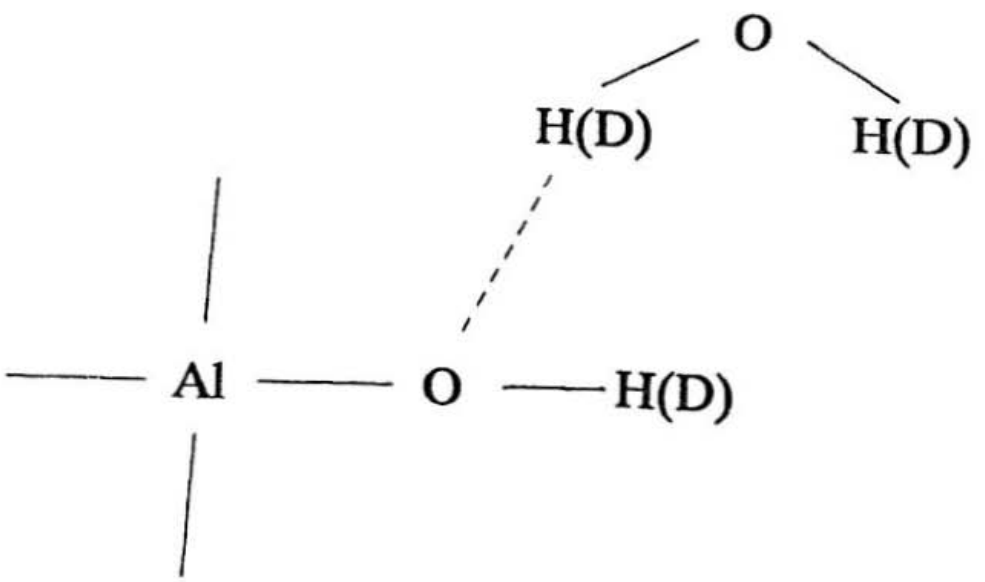

Figure 5.5. Diagrams of Hydrogen Bonding to $Al(OH)_4^-$ or $Al(OD)_4^-$ Species

REFERENCES

1. M. H. Brooker, in The Chemical Physics of Solvation, Part B, edited by R. R. Dogonadze, E. Kalman, A. A. Kornyshev and J. Ulstrup, Chapter 4, p.119, Elsevier, Amsterdam (1986).

2. C. Carr, Spectroscopic Studies of Metal Halide Complexes in Aqueous Solutions, Ph.D. Thesis, Department of Inorganic Chemistry, University of Bristol, England (1984).

3. C. I. Ratcliffe and D. E. Irish, in Water Science Reviews, edited by F. Franks, Vol.3, Chapter 1, p.1, Cambridge University Press, Cambridge (1988).

4. D. E. Irish and M. H. Brooker, in Advances in Infrared and Raman Spectyroscopy, Vol.2, edited by R. J. H. Clark and R. E. Hester, Chapter 6, p.212, Heyden and Son Ltd., London (1976).

5. P. Å. Bergström, Single-ion Hydration Properties in Aqueous Solution - A Quantitative Infrared Spectroscopic Study, Ph.D. Thesis, Institute of Chemistry, Uppsala University, Sweden (1991).

6. P. M. Bertsh, in The Environmental Chemistry of Aluminum, edited by Garrison Sposito, Chapter 2 and 4, p.29 and p.87, Berkeley, California (1989).

7. M. C. Read, On the Hydration of Rh(III) and Cr(III); and the Hydrolysis and Complexation of Rh(III) - An Experimental Study using Diffraction and Spectroscopic Methods, Ph.D.Thesis, Department of Inorganic Chemistry, Royal Institute of Technology, Sweden (1992).
8. M. Magini, G. Licheri, G. Paschina, G. Piccaluga and G. Pinna, X-ray Diffraction of Ions in Aqueous Solutions: Hydration and Complex Formation, CRC Press, Boca Raton, Florida (1988).
9. J. W. Akitt and W. Gessner, J. Chem. Soc. Dalton Trans., 147(1984).
10. R. J. Moolenaar, J. C. Evans and L. D. McKeever, J. Phys. Chem., 74, 20, 3629(1970).
11. M. Liu, Y. Cao, N. Chen and Z. Zhuang, Acta Metallurgica Sinica (English Edition), Series B, 5, 3, 224(1992).
12. N. Chen, M. Liu, Y. Cao, B. Tang and M. Hong, Science in China, Series B, 36, 1, 32(1993).
13. E. R. Lippincott, J. A. Psellos and M. C. Tobin, J. Chem. Phys., 20, 536(1952).
14. C. F. Baes, Jr. and R. E. Mesmer, The Hydrolysis of Cations, John Wiley & Sons, Inc., (1976).
15. G. Johansson, Acta Chem. Scand., 14, 771(1960).
16. H. Ivekovic, T. Vroski and D. Pavlovic, Croatica Chimaca Acta, 28, 1 , 41(1956).
17. M. H. Brooker and P. R. Tremaine, Geochimica Acta, 56, 2573(1992).
18. M. H. Brooker, Proceedings of the International Conference on Raman Spectroscopy, XIII, Würzburg, Germany (1992).
19. A. Smekal, Naturwiss., 11, 873(1923).
20. H. A. Kramers and W. Heisenberg, Z. Phys., 31, 681(1925).

55. K. A. Rodggers, Clay Minerals, 28, 85(1993)
56. Chris Dyer, Patrick J. Hendra, Willis Forsling and Maine Ranheimer, Geochemica, 49A, 5/6, 705(1993).
57. N. N. Greenwood and A. Earnshaw, Chemistry of the Elements, Chapter 7, Pergamon Press, New York, 276(1989).
58. A. R. Davis and G. G. Oliver, Journal of Solution Chemistry, 1, 4, 329(1972).
59. D. E. Irish, D. L. Nelson, and M. H. Brooker, Journal of Chemical Physics, 54, 654(1971).
60. A. D. Buckingham and Liu Fan-Chen, International Reviews in Physical Chemistry, 1, 253(1981).

21. E. Schrödinger, Ann. Phys. (leipzig), 81, 109(1926).
22. P. A. M. Dirac, Proc. Roy. Soc., 114, 710(1927).
23. C. V. Raman and K. S. Krishnan, Nature, 121, 501(1928).
24. G. Landsberg and L. Mandelstamm, Naturwiss., 16, 557(1928).
25. J. M. Stencel, Raman Spectroscopy for Catalysis, Van Nostrand Reinhold, New York, (1990).
26 Recent Trends in Raman Spectroscopy, edited by S. B. Banerjee and S. S. Jha), World Scientific Publishing Co. Pte. Ltd., New Jersey (1989).
27. G L. Eesley, Coherent Raman Spectroscopy, Pergamon Press, New York (1981).
28. Advances in Raman Spectroscopy, Vol.1, edited by M. Jacon, J. -P. Mathieu, Heydon and Son, Lodon (1973).
29. S. S. Jha, Surf. Science 158, 190(1985).
30. Infrared and Raman Spectroscopy, Part A, edited by E.G. Brame, Jr. and Jeanette Grasseli, Marcel Dekker, INC., New York (1976).
31. D. A. Long, Raman Spectroscopy, McGraw-Hill International Book Compan New York (1977).
32. P. R. Bunker, Molecular Symmetry and Spectroscopy, Academic Press (1979).
33. F. A. Cotton, Chemical Applications of Group Theory, Interscience Publishers (1964).
34. J. C. Decius and R. M. Hexter, Molecular Vibrations in Crystals, McGraw-Hill International Book Company, New York (1977).
35. W. G. Fateley, F. R. Doolish, N. T. McDevitt and F. T. Bentley, Infrared and Raman Selection Rules for Molecular and Lattice Vibrations: The Correction Method, Wiley-Interscience, New York (1972).
36. P. Hendra, C. Jones and G. Warnes, Fourier Transform Raman Spectroscopy, Instrumentation and Chemical Application, Ellis Horwood Limited, England (1991).

37. A. Jayaraman, Rev. Mod. Phys., Vol.55, No.1, 65(1983).
38. R. M. Hazen and L. W. Finger, Rev. Sci. Instrum., 52, 1, 75(1981).
39. W. Budde, Physical Detectors of Optical Radiation, Vol.4, of Optical Radiation Measurements, Academic Press, New York (1983).
40. R. K. Chang and M. B. Long, Light Scattering in Solid II, Topics in Applied Physics, Vol.50, edited by M. Cardona and Guntherodt, Springer-Verlag, Berlin, 179(1982).
41. Richard W. Bormett and Sanford A. Asher, Applied Spectroscopy, 48, 1, 1(1994).
42. G. Verdes, R. Gout and S. Castet, Eur. J. Mineral, 4, 767(1992)
43. A. Vogel, Textbook of Quantitative Inorganic Analysis, 4th ed.; Longman, New York (1978).
44. J. K. Hovey, L. G. Hepler and P. R. Tremaine, The Journal of Physical Chemistry, 92, 1323(1988).
45. M. H. Brooker, G. Hancock, B. C. Rice and J. Shapter, J. Raman Spectrosc., 20, 683(1989).
46. J. Pitha and R. N. Johns, Can. J. Chem., 44, 3031(1966).
47. J. Pitha and R. N. Johns, Can. J. Chem., 45, 2347(1967).
48. M. H. Brooker and B. Rice, Chemistry Department, Memorial University of Newfoundland, St. John's, Canada.
49. Thomas M Tuerke et al, Sigma Plot Program, Big Science, AAAS Press, U. S. A., (1993).
50. D. Müller, W. Gessner, H. -J. Behrens and G. Scheler, Chemical Physics Letters, 79, 59(1981).
51. J.W. Akitt, N.N. Greenwood, B.L. Khandelwal and G.D. Lester, J. Chem. Soc., Dalton, 604(1972).
52. D. K. Stephen and W.S. Thomas, Inorg. Chem., 28, 1952(1989).
53. D. Müller, D. Hoebble and W. Gessner, Chem. Phys. Lett. 84, 25(1981).
54. G. Johansson, Acta Chem. Scand., 20, 505(1966).